The University of South Bohemia in České Budějovice Faculty of Science

The energy metabolism of dyskinetoplastic Trypanosoma parasites

Bachelor thesis

Julie Ebenstreitová

Supervisor: RNDr. Alena Panicucci Zíková, PhD
Co-Supevisor: Brian Panicucci

České Budějovice

2023

Ebenstreitová, J., 2023: The energy metabolism of dyskinetoplastic Trypanosoma parasites. Bc. Thesis, in English – 65 p., Faculty of Science, University of South Bohemia, České Budějovice, Czech Republic.

Annotation

Trypanosoma brucei strains that lack their mitochondrial DNA (dyskinetoplastids) are dependent on the reverse activity of the ADP/ATP carrier (AAC) to provide an electrogenic mitochondrial membrane potential ($\Delta\Psi_m$). Since the intensity of the $\Delta\Psi_m$ and the mitochondrial ATP/ADP ratio dictate the direction of the ADP/ATP carrier, we hypothesize that mitochondrial ATP levels will be kept low in these parasites. Therefore, we analyze the $\Delta\Psi_m$ and parasite viability when we stimulate mitochondrial substrate-level phosphorylation in these dyskinetoplastids.

I hereby declare that I am the author of this bachelor thesis, that I have worked independently and used only the sources listed in the bibliography.

České Budějovice, 12.4.2023 ……

Julie Ebenstreitová

Acknowledgment

I would like to thank Alena for giving me the opportunity to become part of the AZ lab and also to participate in such an interesting project, which caught my attention immediately when she talked about it during the lecture and I hoped that she would choose me and no one would be faster. I would also like to thank Brian who guided me through the whole project, with whom we experienced many failures which however led to many successes. He passed on to me his knowledge, experience and most importantly his passion for science. I would like to thank him for all his patience and support. I would also like to thank the members of the AZ lab, especially Martinka, Míša K. and Míša H., who have become my very good friends and colleagues. I am glad for how kindly they welcomed me and whenever there was any problem they always helped me. Last but not least, I would like to thank my family for the motivation during my studies and all the financial help. Special thanks goes to my partner for all the patience and support during the writing of this thesis and for supplying me with my favorite snacks to keep me motivated.

Abbreviations

AAC	ADP/ATP carrier
AAT	African animal trypanosomiasis
ACH	acetyl coenzyme A thioesterase
ADP	adenosine diphosphate
AOX	alternative oxidase
APRT	adenine phosphoribosyltransferase
ASCT	acetate-succinate CoA-transferase
ATP	adenosine triphosphate
BF	bloodstream form
CoA	coenzyme A
DAPI	4',6-diamidino-2-phenylindole
DHAP	dihydroxyacetone phosphate
DIC	differential interference contrast
ETC	electron transport chain
FACS	fluorescence-activated cell sorting
FBS	fetal bovine serum
FCCP	carbonyl cyanide-p-trifluoromethoxyphenylhydrazone
GTP	guanosine triphosphate
GPDH	glycerol-3-phosphate dehydrogenase
HAT	Human African Trypanosomiasis
HRP	horseradish peroxidase
IFA	immunofluorescence assay
kDNA	kinetoplast DNA

LB	lysogeny broth
MM	mastermix
mtHSP70	mitochondrial heat shock protein 70
OXPHOS	oxidative phosphorylation
PAC	puromycin N-acetyl-transferase
PAGE	polyacrylamide gel electrophoresis
PBS	phosphate buffered saline
PBS-G	phosphate buffered saline with glucose
PBS-T	phosphate buffered saline with Tween
PF	procyclic form
PMF	proton motive force
PVDF	polyvinylidene difluoride
SCoAS	succinyl coenzyme A synthetase
SDS	sodium dodecyl sulfate
SOC	super optimal catabolite suppressing broth
TAE	tris-acetate-EDTA
TCA	tricarboxylic acid cycle
TetR	tet repressor
TMRE	tetramethylrhodamine ethyl ester
wt	wild type

Table of content

1. Introduction 1
   1.1. Trypanosomatida 1
   1.2. Trypanosomiasis 1
   1.3. *T. brucei* life cycle 3
   1.4. Metabolism of trypanosomes 4
   1.5. Mitochondrial substrate phosphorylation 6
   1.6. Dyskinetoplastic trypanosoma cell lines 8
2. Aims of the thesis 10
3. Materials and methods 11
   3.1. Cell culture 11
      3.1.1. Cell counting 12
   3.2. Cloning 13
      3.2.1. Genomic DNA isolation 13
      3.2.2. Polymerase Chain Reaction (PCR) 13
      3.2.3. Agarose Gel Electrophoresis 16
      3.2.4. Gel extraction 17
      3.2.5. Restriction digests 19
      3.2.6. Ligation 19
      3.2.7. Transformation 20
      3.2.8. Colony screening by restriction digest 21
   3.3. Western Blot 22
      3.3.1. Whole cell lysate preparations 22
      3.3.2. Gel electrophoresis 23
      3.3.3. Protein transfer 24
      3.3.4. Probing with antibodies 25
      3.3.5. Visualization with ECL on Chemidoc 26
   3.4. Transfection of dyskinetoplastids 26
      3.4.1. Plasmid linearization: 26
      3.4.2. Prepare Trypanosoma culture 27
      3.4.3. Transfection protocol 28
      3.4.4. Selection process 28
   3.5. DAPI staining 29
   3.6. Growth curves 29

3.7. Mitochondial membrane potential 30
3.7.1. TMRE staining 30
3.7.2. Fluorescence measurements on FACS 31
4. Results 31
4.1. Expression levels of enzymes required for the mitochondrial substrate phosphorylation 31
4.2. ASCT protein alignment of *T. brucei* and *T. evansi* 33
4.3. Cloning ASCT into a protein expression plasmid 34
4.3.1. ASCT PCR amplification 34
4.3.2. Restriction digest of the pT7-3V5 plasmid 35
4.3.3. Colony screening of ASCT-pT7-3V5 plasmid 36
4.4. Sequencing of ASCT-pT7-3V5 37
4.5. DAPI verification of dyskinetoplastic cell lines 38
4.6. DK164 pSMOX and *T. evansi* pSMOX ASCT-pT7-3V5 transfections 40
4.7. Growth curves of ASCT dyskinetoplastic cell lines 41
4.8. Verification of ASCT-3V5 expression in *T. brucei* DK164 pSMOX by immunoblotting 42
4.9. Measuring DK164 pSMOX ASCT-pT7-3V5 ΔΨm with TMRE 44
5. Discussion 45
6. References 50

1. Introduction

1.1. Trypanosomatida

Trypanosomatida are unicellular organisms that have a single flagellum and a single mitochondrion (Podlipaev, 2001). All described Trypanosomatids are parasites, usually residing within insects. A few genera are dixenous, meaning they have a life cycle within a secondary host that can be a plant, invertebrate or vertebrate. Several of these dixenous species are human pathogens responsible for some of the worst neglected tropical diseases in the world. One of these is Chagas disease, which is transmitted to humans by Triatomine bugs infected with *Trypanosoma cruzi*. Leishmaniasis is a disease caused by various *Leishmania* species found in the tropics, subtropics, and southern Europe. These parasites are transmitted by phlebotomine sand flies (Kaufer et al., 2017). Finally, the etiological agent of Human African Trypanosomiasis (HAT) is *Trypanosoma brucei brucei,* which is transmitted by tsetse flies (Simpson et al., 2006). Notably, of all the Trypanosomatids, only *Trypanosoma brucei brucei* is an extracellular parasite.

1.2. Trypanosomiasis

HAT, also known as African sleeping sickness, is caused by two subspecies of trypanosomes, *Trypanosoma brucei gambiense* and *Trypanosoma brucei rhodesiense*. These parasites are transmitted by tsetse flies (*Glossina* species) that are geographically restricted to sub-Saharan Africa (area highlighted in yellow on Figure 1). Interestingly, the disease propagated by *Trypanosoma brucei gambiense* and *Trypanosoma brucei rhodesiense* is different. While the distribution of *Trypanosoma brucei rhodesiense* is confined to a few rural areas in Eastern Africa, it causes an acute form of the disease that is more virulent compared to the chronic disease manifestation caused by *Trypanosoma brucei gambiense* in Western Africa (Figure 1). While the disease is often lethal if untreated, new drugs like fexinidazole and acoziborole are proving to be highly effective (Dickie et al., 2020). This combined with active government programs that control tsetse populations located in close proximity to urban areas has resulted in a dramatic reduction in the number of infections in recent years. While there were an estimated 300,000 infected individuals in 1995, there were only 1,000 reported cases in 2019 (https://www.who.int). This trend is a very positive outcome of renewed attention to HAT in the last 20 years, but the population at risk of HAT includes 70 million people in 36

countries if the parasites develop resistance to the drugs or renewed war or increased poverty curtail government programs.

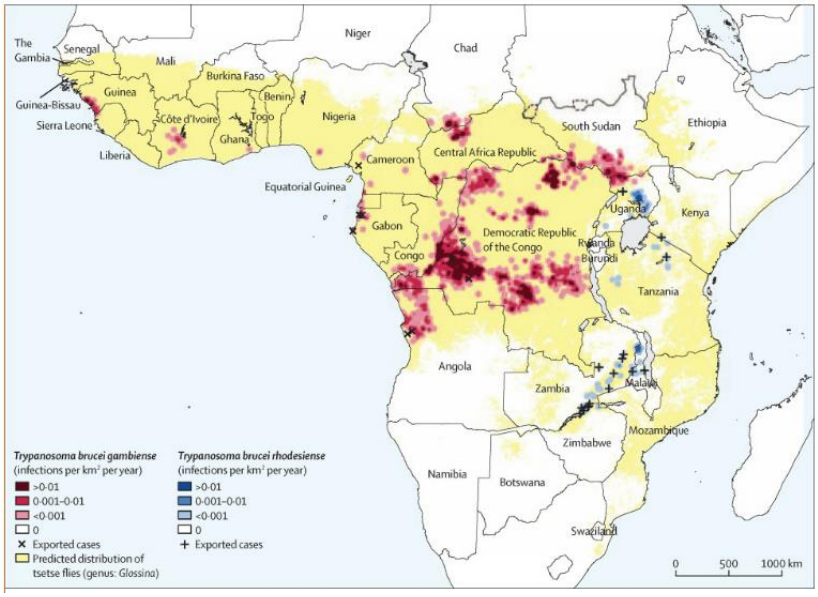

Figure 1: Geographical distribution of cases of Human African Trypanosomiasis (HAT) caused by *Trypanosoma brucei gambiense* and *Trypanosoma brucei rhodesiense*. The area marked in yellow represents the occurrence of tsetse flies (*Glossina* species). Adapted from Büscher et al., 2017.

A far bigger economical burden is imposed by African animal trypanosomiasis (AAT). Also known as Nagana, it affects both domestic and wild animals. Infected animals suffer from fever, weakness, lethargy and anaemia, resulting in weight loss, lower fertility, less milk production and eventual death (https://www.gla.ac.uk). Due to these diseases, the African economy is negatively affected, costing an estimated five billion dollars in lost animal productivity (Swallow, 2000). AAT is transmitted by various *Glossina* species of tsetse flies that are infected with *Trypanosoma congolense*, *Trypanosoma vivax*, and *Trypanosoma brucei brucei*. Currently, the only treaments of AAT include diminazene aceturate, isomethamidium chloride, and ethidium bromide. However, diminazene and isometamidium are only effective at early stages of the disease. Furthermore, due to poor protocols outlining AAT treatment that are often implemented by the farmers themselves, it is increasingly common for parasites to demonstrate drug resistance (Okello et al., 2022).

1.3. *T. brucei* life cycle

Since *Trypanosoma brucei brucei* cannot infect humans and its genome can be easily altered, it has been subjected to extensive research for decades. Thus, it is considered a model organism for African trypanosomes (Horn, 2022). From here on in, *Trypanosoma brucei brucei* will be referred to as simply *T. brucei*.

T. brucei has a complex life cycle that alternates between a mammalian host and an insect vector. As it encounters various environments, it adapts and transforms into several different developmental stages (Zíková, 2022). During the early phase of mammalian infection, *T. brucei* has a long slender morphology and divides rapidly (Figure 2). Since the extracellular parasite resides in the bloodstream, it must rapidly exchange its surface protein coat to evade host defence mechanisms (Mugnier et al., 2016). Once the parasitemia reaches a critical cell density, *T. brucei* differentiates into a short stumpy form that is specialized for transmission into the tsetse fly. This developmental stage no longer divides, presumably prolonging the mammalian infection until another tsetse fly can take a bloodmeal (Matthews, 2021). When the trypanosomes enter and colonize the fly midgut, they undergo morphological and metabolomic changes to become procyclic trypomastigotes. During their migration through the proventriculus, they again differentiate into epimastigotes that undergo a single asymmetric division. Next, they proceed to the salivary glands, where they attach and begin to divide. Some of these epimastigotes will then detach and transform into non-dividing metacyclic parasites that are ready for transmission into a new mammalian host (Langousis & Hill, 2014; Silvester et al., 2017). Until recently, it was only possible to cultivate the long slender bloodstream forms (BF) and the procyclic form (PF) trypomastigotes in flasks for extended periods of time. Since most of the discovered *T. brucei* biology originated from these two life cycle stages, from this point we will refer to them as BF and PF for reasons of brevity.

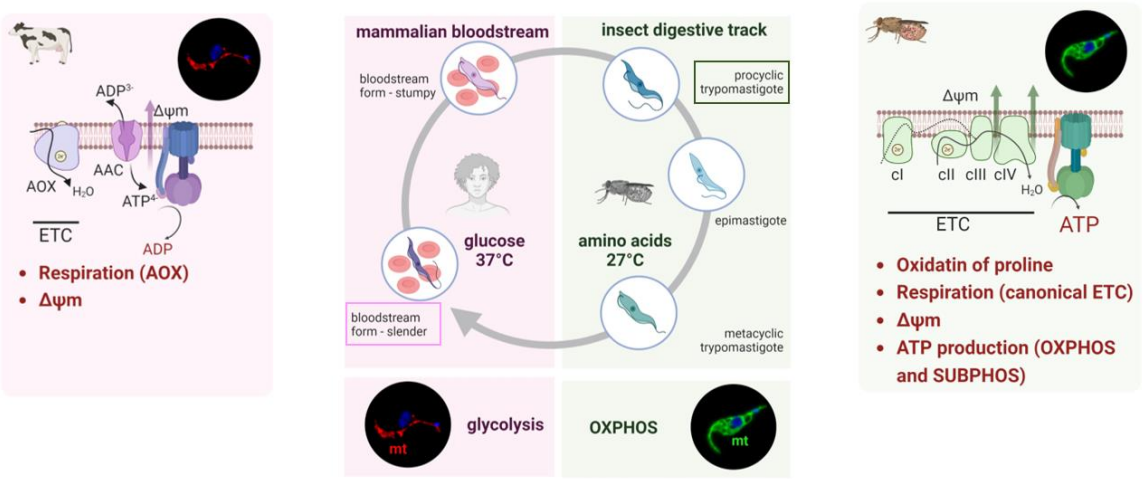

Figure 2: Differences between the procyclic form (PF) and the bloodstream form (BF) *T. brucei* life cycle stages. The pink background represents BF parasites, which live at 37 °C in the glucose-rich mammalian bloodstream, where they can generate sufficient ATP by glycolysis. The green background represents PF *T. brucei*, which live at 27 °C in an amino acid-rich environment in the tsetse fly, where they generate ATP by oxidative phosphorylation.

1.4. Metabolism of trypanosomes

As *T. brucei* encounters various environments throughout the progression of its life cycle, it must adapt its metabolism to the nutrients available. Therefore, as a metabolic hub, the mitochondrion undergoes drastic metabolic and structural remodelling during the parasite's programmed differentiation. The highly-branched mitochondrion observed in PF are rich in invaginations of the inner mitochondrial membrane that form cristae. These cristae increase the surface area of the membrane and provide a microenvironment that supports adenosine triphosphate (ATP) production during oxidative phosphorylation (Verner et al., 2015). Indeed, PF have a canonical electron transport chain (ETC) where respiratory complexes III and IV accept electrons and pump protons across the inner mitochondrial membrane and into the intermembrane space (Figure 2 & 3). The F_oF_1-ATP synthase utilizes the potential energy of this proton motive force to generate chemical energy in the form of ATP. To meet the energy demands of the entire cell, this ATP generated in the mitochondrial matrix needs to be transported into the cytosol by the ADP/ATP carrier (AAC). This exchange of a mitochondrial ATP for a cytosolic ADP is reversible depending on the bioenergetic properties of the mitochondria. It is important to note that in the tsetse fly, the most abundant carbon sources for *T. brucei* are threonine and proline (Mantilla et al., 2017). The catabolic pathways of these two

amino acids leads to the production of NADH and FADH, respectively. These two cofactors are then used as electron sources for the ETC.

In contrast, the tubular BF mitochondrion is simplified, retaining only a few cristae that are reduced in size (Bílý et al., 2021). Despite these changes, the function of the mitochondrion is still required for the survival of the BF trypanosome (Zíková et al., 2017). However, this developmental stage of the parasite lacks a canonical ETC. Instead, respiration occurs through the mitochondrial glycerol-3-phosphate dehydrogenase (GPDH) and an alternative oxidase (AOX) (Figure 2 & 4). While neither of these enzymes pump protons across the inner mitochondrial membrane, they do help to maintain the redox balance in the glycosome, which are specialized peroxisomes that contain the first 9 enzymes of glycolysis. This redox balance occurs via the dihydroxyacetone phosphate (DHAP)/glycerol-3-phosphate shuttle. During this process, the mitochondrial GPDH transfers its electrons to ubiquinone to generate ubiquinol (Michels et al., 2021). These electrons from ubiquinol are then transferred to oxygen by AOX, thereby reducing oxygen to water (Chaudhuri et al., 2006).

Without functional respiratory complexes III and IV to pump protons, the F_oF_1-ATP synthase reverses to hydrolyze ATP and maintain the mitochondrial membrane potential ($\Delta\Psi_m$) (Schnaufer et al., 2005). This ATP synthase activity allows the enzyme to pump protons from the matrix into the mitochondrial intermembrane space. This sustained F_oF_1-ATP synthase activity is unique in BF *T. brucei*, but is essential for the parasite because the $\Delta\Psi_m$ is required for mitochondrial protein import. The inability to produce large amounts of ATP by oxidative phosphorylation would be detrimental to most cells, but luckily the extracellular parasite resides in the glucose-rich bloodstream of the mammalian host. Due to the compartmentalization of glycolysis in the glycosomes, BF *T. brucei* is able to produce enough cellular ATP even via the inefficient pathway of glycolysis, which generates only 2 ATP per glucose molecule compared to the 32 ATP synthesized by oxidative phosphorylation (Allmann & Bringaud, 2017).

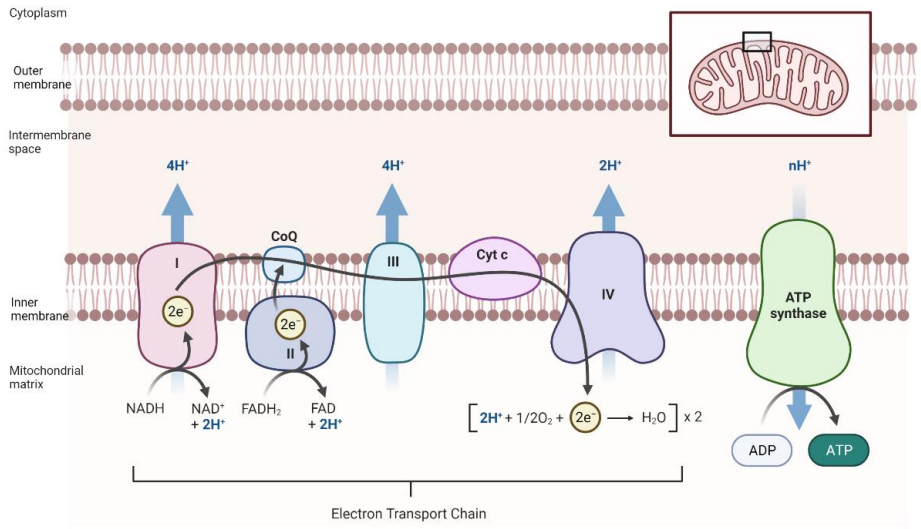

Figure 3: Process of canonical oxidative phosphorylation including electron transport chain (ETC) and ATP synthase. On the inner membrane of the mitochondrion is a group of respiratory complexes (I to IV) that comprise the electron transport chain (ETC). Protons can be pumped into the mitochondrial intermembrane space by complexes, I, III and IV to form an electrochemical gradient. The potential energy of the proton motive force is used by the F_OF_1-ATP synthase (complex V) to generate ATP. Schematic generated using BioRender.

1.5. Mitochondrial substrate phosphorylation

The majority of ATP in the PF *T. brucei* is produced by ATP synthase in the mitochondrion. However, there is also a significant amount of mitochondrial ATP generated by substrate-level phosphorylation. In this process, ATP is created when an enzyme transfers a phosphate group from a donor substrate to adenosine diphosphate (ADP). While glycolysis is a classic example of substrate-level phosphorylation, this process occurs in the glycosome and cytoplasm of the parasite. Instead, substrate-level phosphorylation can occur via one of two unique metabolic pathways in the *T. brucei* mitochondrion (Bochud-Allemann & Schneider, 2002) (Figure 4). The first route involves succinyl-CoA synthetase (SCoAS), which is part of the tricarboxylic acid (TCA) cycle. In a typical mitochondrion, acetyl coenzyme A (acetyl-CoA), a product of glucose oxidation, enters the TCA cycle and is further oxidize to generate CO_2 and NADH, a reducing agent that donates electrons to the ETC. During this cycle, SCoAS converts succinyl-CoA to succinate, completing the decarboxylation of pyruvate. This reaction can either generate a molecule of guanosine triphosphate (GTP) or ATP (Williams, 2022). In most eukaryotes, the enzyme has a preference for GTP, but the *T. brucei* SCoAS prefers ATP. The enzyme is a heterodimer comprised of an alpha and beta subunit. The alpha subunit

contains a Rossman fold that binds coenzyme A, while the beta subunit has an ATP grasp domain where the nucleoside triphosphate is formed.

The *T. brucei* mitochondrion has a second substrate-level phosphorylation pathway that involves the generation of acetate from acetyl-CoA (Rivière et al., 2009). Some pyruvate produced from glycolysis is transported into the mitochondrion where it is converted to acetyl-CoA. There are two different metabolic pathways that can convert this acetyl-CoA into acetate. The first route utilizes the enzyme acetyl-CoA thioesterase (ACH), but this reaction does not generate ATP. The second pathway employs the enzyme acetate-succinate CoA-transferase (ASCT), an enzyme normally found only in anaerobic organisms (Van Hellemond et al., 1998). Importantly, ASCT cooperates with SCoAS to produce ATP in the ASCT/SCoAS cycle. The ASCT-SCoAS cycle can also be utilized in the formation of acetyl-CoA by conversion from threonine, which BF trypanosomes also metabolize, to produce ATP (Figure 4) (Mazet et al., 2013; Mochizuki et al., 2020).

For a long time, it was thought that the mitochondrion in BF *T. brucei* was exclusively an ATP consumer since the F_oF_1-ATP synthase functions in reverse to hydrolyze ATP and pump protons into the mitochondrial intermembrane space. In this model, the AAC reverses and transports cytosolic ATP produced via glycolysis into the mitochondrion to supply the substrate for the ATP synthase activity. However, the Zíková lab found that compared to PF *T. brucei*, the BF parasites are drastically less sensitive to the AAC inhibitor carboxyatractyloside. Indeed, recent studies in the lab demonstrate that BF *T. brucei* survive just fine without the AAC. Lacking any other active mitochondrial ATP transporter, it was shown that the BF mitochondrion can produce their own ATP by substrate phosphorylation using SCoAS (Husová, 2021).

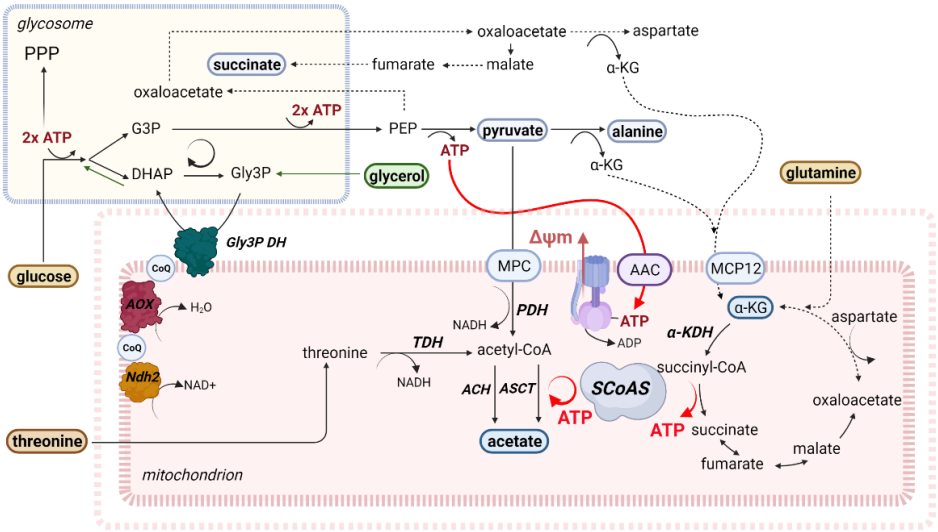

Figure 4: Illustration of the different metabolic pathways in the bloodstream from (BF) *T. brucei*. Metabolic pathways occurring in the glycosome are shown in a yellow background and pathways occurring in the mitochondrion are shown in a pink background (generated using BioRender).

1.6. Dyskinetoplastic trypanosoma cell lines

One of the most obvious features of Trypanosomatids when viewed by electron microscopy is the dense network of the mitochondrial DNA. Before it was known what the structure was composed of, its close proximity to the base of the flagellum resulted in the name kinetoplast. The mitochondrial genome that makes up the kinetoplast consists of two types of circular DNA, dozens of maxicircles and thousands of minicircles (Shlomai, 2004). Maxicircles resemble most eukaryotic mitochondrial genomes in that they encode the mitoribosomal RNA and a few of the very hydrophobic subunits of the large protein complexes involved in oxidative phosphorylation or the mitoribosome. However, the majority of the maxicircle genes are cryptogenes that once transcribed into RNA must be extensively edited by the insertion or deletion of uridines to create functional gene products (Stuart et al., 2005). This complex process involves the guide RNAs encoded on the minicircles that direct the uridine insertion/deletions by the editosome complex (Carnes et al., 2015).

There is a group of trypanosomes that lack all (akinetoplastic) or important components (dyskinetoplastic) of their kinetoplast DNA (kDNA) that does not allow for the proper editing of the mitochondrial transcripts. The loss of kDNA locks trypanosomes in the BF stage of their life cycle because they are no longer able to utilize the amino acids available in the tsetse fly to perform oxidative phosphorylation and generate ATP (Borst & Hoeijmakers, 1979; Schneider,

2001). Since dyskinetoplastids can no longer infect tsetse flies, they must now rely on the mechanical transmission between mammalian hosts by biting flies. This allows dyskinetoplastic trypanosomes to leave the African tsetse belt and spread to other continents, making them the pathogenic trypanosomes with the widest geographic distribution (Carnes et al., 2015).

Dyskinetoplastic cell lines include *Trypanosoma evansi* AnTat3/3 *(T. evansi)* and *Trypanosoma equiperdum* (*T. equiperdum),* which are closely related to *T. brucei*. *T. evansi* primarily infects camels and horses, causing a disease called surra (Figure 5). This is of great economic importance in Africa, Asia and South America, where thousands of animals die annually from infection (Desquesnes et al., 2013). *T. equiperdum* infects mainly horses and causes a disease called Dourine (Claes et al., 2005). Dourine is endemic in some African, Asian and Latin American regions, as well as the Middle East and Eastern Europe. However, there are some differences between these dyskinetoplastic species. Both have abnormal networks, but *T. evansi* cannot develop fully functional mitochondrion because they completely lack a maxicircles, so they do not have the necessary gRNAs to perform RNA editing, but they still retain a single class of minicircles that lacks the sequence heterogeneity typical of *T. brucei* (Borst et al., 1987). In contrast, *T. equiperdum* have maxicircles and homogeneous minicircles (Lun et al., 1992). Another representative of the dyskinetoplastids is *Trypanosoma brucei* EATRO164 (DK164), which does not occur in nature. It was created in the laboratory by repeated exposures to the carcinogen acriflavine, a fluorescent dye that intercalates between nucleotide base pairs in the DNA. The DK164 lacks all kinetoplast DNA, but retains the editosomes required for mitochondrial RNA editing (Domingo et al., 2003).

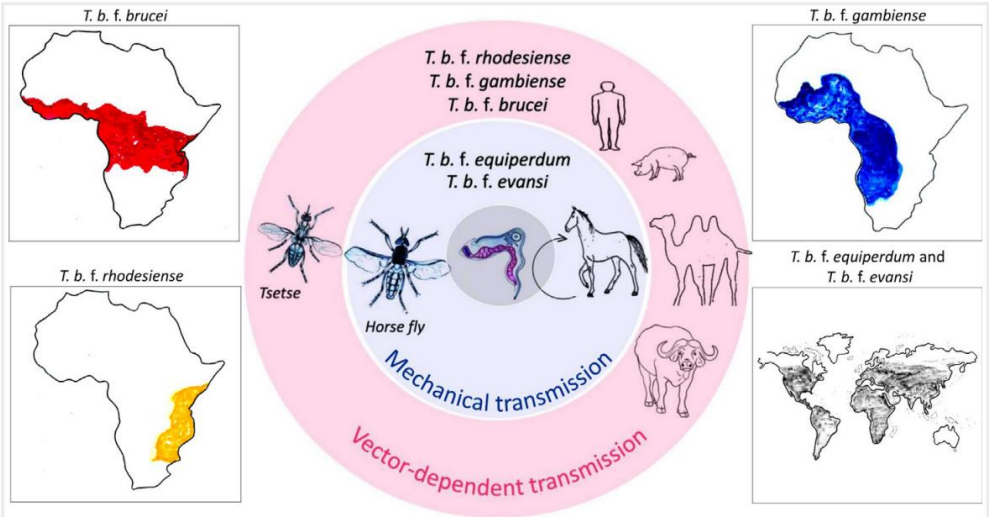

Figure 5: Overview of the two main transmission mechanisms that distribute various *T. brucei* subspecies throughout the world. The pink circle represents trypanosomiasis

transmission that is tsetse fly dependent and is therefore geographical restricted to Africa. The blue circle represents *T. brucei* species that cannot infect insects and therefore must be transmitted mechanically by biting flies. This independence from *Glossina* species means that its geographical distribution is not limited to Africa. Adapted from Lukeš et al., 2022.

Crucially, due to the non-canonical ETC employed by the BF *T. brucei*, there is basically only a single mitochondrial gene product required for the viability of the parasite. This gene encodes for subunit *a* of the F_oF_1-ATP synthase, which along with the hydrophobic c-ring, creates a proton pore through which the protons can pass through the mitochondrial inner membrane by rotating the F_oF_1-ATP synthase. The incorporation of this mitochondrial encoded subunit into the F_oF_1-ATP synthase allows the enzyme to maintain the essential $\Delta\Psi_m$ by pumping protons into the intermembrane space. The dyskinetoplastic parasites are able to survive in the mammalian host because they have altered their bioenergetics to maintain the $\Delta\Psi_m$ even without a fully functional F_oF_1-ATP synthase. To compensate, they rely on the electrogenic charge provided by AAC when it exchanges a cytosolic ATP^{4-} for a mitochondrial ADP^{3-}. This results in a +1 charge in the intermembrane space that is sufficient to generate an electrogenic membrane potential for protein import (Šubrtová et al., 2015). In order to maintain this high flux of ATP import by the reverse mode of AAC, the mitochondrial ATP pool must be kept low. While the F_oF_1-ATP synthase is not able to pump protons in dyskinetoplastids, it can still hydrolyze mitochondrial ATP (Dean et al., 2013). In this manner, the AAC and ATP synthase activity maintains the $\Delta\Psi_m$. To keep this process running, we believe that mitochondrial substrate-level phosphorylation must be limited in the dyskinetoplastic parasites so that the mitochondrial ATP pool does not become inhibitory. To test this hypothesis, we overexpressed ASCT in DK164 and *T. evansi* dyskinetoplatids in order to stimulate the activity of the ASCT/SCoAS cycle.

2. Aims of the thesis

The main aims of this thesis are as following:

1. Perform DAPI staining to verify that the dyskinetoplastic cell lines truly lacked mitochondrial DNA.
2. Determine the expression levels of various proteins involved in trypanosoma bioenergetics by immunoblotting.
3. Generate dyskinetoplastic parasites that overexpress acetate:succinate CoA-transferase

4. Analyze how this expression affects parasite viability and the mitochondrial membrane potential

3. Materials and methods

3.1. Cell culture

BF *T. brucei* Lister 427 wt and the dyskinetoplastic *T. brucei* EATRO164 DK and *T. evansi* AnTat 3/3 wt cell lines were used for this project. The two wild type strains represent the parasite as it is found in nature, while the DK164 cell line is a mutant lacking mitochondrial DNA that was created in the lab by repeated exposures to the carcinogen acriflavine, a fluorescent dye that intercalates between nucleotide base pairs in the DNA. Two additional cell lines derived from *T. brucei* EATRO164 DK and *T. evansi* AnTat 3/3 wt were also used for inducible gene expression. The *T. brucei* EATRO164 DK pSMOX (DK164 pSMOX) and *T. evansi* AnTat 3/3 pSMOX (*T. evansi* pSMOX) cell lines were genetically modified with the integrated pSMOX plasmid that encodes the constitutive expression of the Tet Repressor (TetR) and the T7 RNA polymerase. The T7 RNA polymerase, originating from the T7 bacteriophage, transcribes DNA downstream from a T7 promoter sequence. TetR is a bacterial protein that binds the Tet DNA operon. In the presence of the antibiotic tetracycline, the TetR undergoes a conformational change and is released from the Tet operon. Under this genetic system, ASCT expression can be induced with tetracycline because its expression plasmid contains an upstream T7 promoter followed by the Tet operon. Therefore, in the absence of tetracycline, the TetR physically impedes the procession of the T7 RNA polymerase. When tetracycline is added to the culture, transcription is allowed to proceed.

The BF *T. brucei* and *T. evansi* cell lines were grown in HMI-11 medium supplemented with 10% fetal bovine serum (FBS). This medium was prepared using a premixed powder. The pH was adjusted to 7.3 using 10M NaOH since this is the physiological pH of the parasites. Phenol red, a colorimetric pH indicator, was included in the medium. It has a yellow to red color range and can help detect if something is wrong with the cells. At a pH around 7, the color of the medium is more red. However, when the culture becomes overgrown, the medium changes to a more yellowish color due to all the lactic acid excreted from the parasites. The medium is stored at 4 °C, but must be pre-warmed in a 37 °C incubator before being applied to the cultures, otherwise the parasites will be stressed due to the temperature shock. The genetically modified DK164 pSMOX and *T. evansi* pSMOX cell lines are grown in medium

containing 100 ng/ml of the antibiotic puromycin. Since the pSMOX plasmid encodes puromycin N-acetyl-transferase (PAC), which degrades puromycin, the presence of the antibiotic acts to positively select only those parasites harboring the pSMOX plasmid.

Cells were grown in 25^2 cm flask and kept between 5 to 10 ml of total volume. The growth of the culture would be limited in larger volumes because of decreased oxygenation, while lower volumes are more susceptible to evaporation. Since the parasites are grown in a 37 °C incubator with 5% CO_2, the lids of the flasks were left slightly loose to facilitate the interaction of CO_2 with the medium. This is important because the medium contains sodium bicarbonate, which acts as a weak pH buffer at physiological values when in equilibrium with CO_2. In order to prevent the cultures from becoming overgrown and stressed, they were split with fresh medium when the cell density of the culture reached 1-2 x 10^6 cells/ml. BF *T. brucei* have a doubling time of about 8 hours, while dyskinetoplastic parasites have a slightly longer doubling time. If the cultures were just being maintained, they could be split "to nothing" every two days since their growth rate is not affected at these lower cell densities. In this scenario, all but the last few drops of culture were removed and replaced with new HMI-11 medium. If a dense culture was needed for the next day, cells were divided 1:10 (i.e. all but 1 ml of culture was removed before adding 9 ml of fresh medium). The health of the cultures was monitored regularly by observing the density, mobility and morphology of the parasites under a light microscope.

3.1.1. Cell counting

In order to keep the culture growing at mid-log phase, it is important to accurately count the cell density before seeding the cell culture. Luckily, mobile trypanosomatids remain in suspension and the cell density can easily be calculated with the Z2 Coulter counter (Beckman Coulter Inc.). The basic principle of the machine is that the parasites pass single file through an electrode and a cell is counted when the current drops (Neikov & Yefimov, 2019). Before counting, the parasites need to be chemically fixed to render them non-infectious while maintaining their morphology. Therefore, 100 µl of cell culture was added to 100 µl of the Trypanosomatid Cell Fix Solution (Table 1) and mixed well. 50 µl of fixed cells were placed in prepared cuvettes filled with 5 ml of Hemasol, the conductive diluent. These cuvettes were inserted into the counter one at a time so that the aperture of the probe was completely immersed in the hemasol. With the dilution factor of the parasite sample entered into the computer, the cells were counted and the cell density of the culture was calculated.

Table 1: Trypanosomatid Cell Fix Solution.

Reagent	Amount	[Final]
dH_2O	85 ml	
SSC	5 ml	1x
Formaldehyde	10 ml	3.6%
TOTAL VOLUME	100 ml	

3.2. Cloning

3.2.1. Genomic DNA isolation

The isolation of *T. brucei* genomic DNA is the first process of cloning since it will serve as the template to amplify the ASCT gene during PCR. This process was performed using the commercial kit Exgene TM Clinic SV by GeneAll. It enables the rapid and pure isolation of genomic DNA from a variety of sample types. First $1x10^8$ parasites were harvested and resuspended in 200 µl of the commercial CL buffer. Since genomic DNA is tightly wound around histone proteins, 20 µl of the serine protease Proteinase K was added to digest the proteins and release the DNA. Then 200 µl of BL buffer was added to lyse the cells. Everything was mixed thoroughly and incubated at 56 ℃ for 10 minutes. Then, 200 µl of absolute ethanol was added to precipitate the DNA. This mixture was transferred to a prepared spin column and centrifuged at 6,000 xg for 1 minute. The flow-through liquid was discarded and the membrane with the genomic DNA was washed with two buffers containing alcohol to remove excess salts. First, 600 µl of the commercial BW buffer was added and the column was centrifuged for 1 minute at 6,000 xg. The second wash included 700 µl of the TW buffer and a spin for 1 minute at 6,000 xg. The flow-through liquid was again discarded. The DNA was then eluted by incubating the membrane with 50 µl of the AE buffer warmed to 60 ℃ for 1 minute before the column was centrifuged at full speed (>12,000 xg) for 1 minute. The DNA concentration is then measured using the NanoDrop 1000 Spectrophotometer (Thermo Scientific). In order not to shear the complex genomic DNA with ice crystals, the sample is stored at 4 ℃.

3.2.2. Polymerase Chain Reaction (PCR)

PCR is a method used to amplify many copies of a specific segment of the genome using DNA fragments called primers that define the concrete region that will be amplified (https://www.genome.gov). PCR was performed using the KOD Hot Start DNA Polymerase kit (Novagen). The KOD Hot Start DNA Polymerase is a proofreading enzyme that very precisely

amplifies genomic or plasmid DNA up to 20 kbp. When the polymerase recognizes that it has inserted a nucleotide that is not correctly based paired with the template, its strong 3'→5' exonuclease activity will remove the incorrect nucleotides and start the 5'→3' replication process again (https://www.merckmillipore.com).

A standard PCR reaction was assembled in a 200 µl thin-walled PCR tube according to the manufacturers suggestion (Table 2) to a 1.5 ml tube. If there are multiple samples with similar components, creating a mastermix (MM) helps with uniformity and saves time pipeting. The volume of each component in the MM is calculated by multiplying the volume in the standard reaction by the number of samples needed. The resulting MM is then aliquoted into each PCR tube. Next, a specific volume of the template DNA is added to this tube. The amount added is calculated from the DNA concentration and the type of DNA: 200 ng for genomic DNA or 10 ng for plasmid DNA. If too much template is used, the reaction may fail because of the concentration-dependent denaturation of the template. PCR grade water is then added to these tubes to give a final volume of 50 µl.

Table 2: PCR setup.

Component	Amount	[Final]
10X Buffer for KOD Hot Start DNA Polymerase	5 µl	1X
25 mM MgSO4	3 µl	1.5 mM
dNTPs (2 mM each)	5 µl	0.2 mM (each)
PCR Grade Water	X µl	
Sense (5') Primer (10 µM)	1.5 µl	0.3 µM
Anti-Sense (3') Primer (10 µM)	1.5 µl	0.3 µM
Template DNA	Y µl	
KOD Hot Start DNA Polymerase (1 U/µl)	1 µl	0.02 U/µl
TOTAL VOLUME	50 µl	

The tubes were placed in the T100^{TM} Thermal Cycler (Bio-Rad) and each PCR step was entered on the computer touch screen (Table 3). The polymerase activation, denaturation, and extension time were based on the recommendations of the DNA polymerase manufacturer. The length of the extension time was calculated from the longest predicted amplicon size. The annealing temperature is the experimental variable that may need to be optimized for the primers used in the reaction. A lower value with generate non-specific amplification of DNA, while higher temperatures may prevent efficient primer annealing. While the annealing temperature is influenced by the predicted melting temperature of the primers, a common

starting value of 52 ℃ is typically used in the lab. Meanwhile, the number of program cycles required to generate the desired amount of PCR product depends on the type and amount of template DNA. A wide range between 20 and 40 cycles is recommended. However, for plasmid DNA, typically only 20 to 25 cycles are sufficient due to the low DNA complexity. A greater number of cycles (~30-35) is suggested for genomic DNA because of the low representation of the targeted sequence within the large genome.

Table 3: PCR cycling conditions.

Step	Target size	
	1000–3000 bp	**> 3000 bp**
1. Polymerase activation	95°C for 2 min	95°C for 2 min
2. Denature	95°C for 20 s	95°C for 20 s
3. Annealing	Lowest Primer T_m°C for 10 s	
4. Extension	70°C for 20 s/kb	70°C for 25 s/kb
Repeat steps	20–40 cycles	20–40 cycles

2.2.2.1. Primer design

Primer design is a critical step for PCR success. The optimal length of the primer is about 18-30 bases; if there are fewer bases, it can lead to the amplification of non-specific PCR products. For a moderate melting temperature, the proportion of guanine (G) and cytosine (C) in the primers should be the same as those of adenine (A) and thymine (T). The design of the forward and reverse primer pair is very important for primer annealing, which determines the specificity and sensitivity of the PCR. The forward primer, which binds to anti-sense strand of the template DNA, should contain the start codon ATG when the gene of interest is not expressed in a plasmid that encodes an N-terminal tag or start methionine residue (https://sharebiology.com). The reverse primer should contain a stop codon if no C-terminal tag is incorporated in the expression plasmid. In order to clamp down the end of each primer, it is best if the 3‘ end is a G or C nucleotide that base pairs with three hydrogen bonds. To avoid primer dimer formation, primer pairs should be checked for complementarity.

To stitch our amplified ASCT gene into our expression plasmid, the 5‘ end of each primer will contain a restriction site that will produce an overhang that is complementary to the same overhang in the digested plasmid. Restriction enzymes, which are proteins isolated from bacteria that cleave DNA molecules at specific sites. The enzymes Nco I (CCATGG) or Nde I

(CATATG) are often used because they include an ATG that can encode the N-terminal methionine residue if it is cloned in frame with the rest of the gene coding sequence. Restriction enzymes need to bind the DNA before they can cleave the molecule, so it is advisable to extend the 5' end of the primer by 3-4 random nucleotides to increase enzyme efficiency. For gene expression plasmids, it is important to insert the amplicon in the correct orientation. To ensure this, a different restriction site must be used in the forward and reverse primers. Downstream of the restriction site, the 3' end of the primer will contain the complementary sequence to the gene of interest. This overlap should be long enough to provide sequence specificity, which is generally about 20 nucleotides (General guidelines for primer design, 2015).

3.2.3. Agarose Gel Electrophoresis

Electrophoresis is a method in which molecules, such as DNA, are separated on the basis of their size and electrical charge in the presence of an electric current. Since the phosphate backbone of DNA is negatively charged, individual molecules move from the negatively charged cathode to the positively charged anode. The crosslinking of the agarose polymers in the gel creates a matrix with uniformly sized pores that the DNA molecules must traverse. Therefore, shorter molecules migrate faster than longer ones because they pass through the gel more easily (https://www.khanacademy.org). The size of the pores in the gel are proportional to the percentage of the agarose in the gel. The higher the percentage of agarose, the smaller the pore size. Therefore, the amount of agarose is selected depending on the size of the amplicon. Typically, a 0.8% agarose gel is selected for bands greater than 3000 bp, while agarose of gels of 1% and 1.2% are used to resolve bands between 3000-1000 bp or less than 1000 bp. Once the percentage of agarose is decided, the weight of the agarose is calculated based of the desired volume of the solvent TAE (Tris-acetate-EDTA). The total volume of the gel is one of the variables that dictates the volume of each well and how much sample can be loaded. In general, an agarose gel with a total volume of 70 ml is warmed for 1 minute in the microwave. The glass Erlenmeyer flask is then swirled slightly to distribute the heat evenly. The flask is then microwaved for another 20 seconds to dissolve the remaining pieces of agarose. To visualize the DNA molecules, the gel needs to be stained with ethidium bromide, a fluorescent dye that intercalates double-stranded DNA. For environmental reasons, we add the carcinogen agent directly to the agarose before it solidifies. However, ethidium bromide is heat labile, so the flask must first be cooled under a cold stream of water until it can be touched with the bare hand. Then 1 µl of Ethidium Bromide is added and mixed by gentle swirling so as not to introduce too many bubbles. The agarose gel is poured into a tray with two casting

dams at either end. A comb to create the sample wells is inserted at one end of the gel. A comb, which comes in a variety of thickness and number of wells, is selected based on the number and volume of the samples to be loaded. After removing any bubbles with a pipette tip, the gel is left for approximately 30 minutes to allow it to completely cool down and solidify. After this time, the comb and casting dams can be carefully removed and the gel is transferred into the buffer tank.

The buffer tank consists of positive (red) and negative (black) electrode at each end, which creates a voltage gradient through the TAE buffer that submerses the agarose gel. Gel electrophoresis takes approximately 1 hour, depending on the percentage of agarose gel, the voltage applied and the expected fragment size. A constant voltage of 90 to 110 V is typically applied to the gel. If the DNA samples contain a complex mixture of various sized fragments that are similar in size, they need to be resolved on the gel for a longer period of time. This also applies to DNA molecules of very large size. The DNA samples contain a 10x DNA loading dye to visualize the leading edge of the migration (Table 4). Once the electrophoresis is complete, the DNA fragments in the gel can be visualized with a UV light and camera housed in the ChemiDoc (Bio-Rad).

Table 4: Composition of the 10x DNA loading dye.

Reagent	[Stock]	Amount	[Final]
MilliQ		4.2 ml	
Glycerol	80%	4.9 ml	39%
SDS	10%	500 µl	0.5%
EDTA	0.5 M	200 µl	10 mM
Xylene cyanol	2%	250 µl	0.1%
TOTAL VOLUME	10 ml		

3.2.4. Gel extraction

Depending on the specificity of the PCR primers and the annealing temp, more than a single molecule of DNA may be amplified. The use of agarose gel electrophoresis allows us to separate our amplicon of expected size from the other nonspecific DNA molecules, which include the abundant primers that were incorporated during the PCR. However, our DNA needs to be extracted from the gel before it can be further manipulated during downstream cloning events. In the lab, we use the GenElute™ Gel Extraction Kit (Sigma-Aldrich), which ensures very accurate and fast purification of linear DNA or plasmids up to 10 kb.

The first step of the gel extraction involves separating the DNA fragment from as much of the agarose as possible. The DNA visualization occurs when the gel is placed on an exposed UV light box. Therefore, personal protective equipment such as a face shield and gloves must be worn as the UV light can severely damage the skin or eyes by burning them. Using a razor blade, care is taken to excise the desired DNA fragment with as little agarose gel as possible. are taken and it is transferred to a 1.5 ml tube. It is necessary to work quickly in order to reduce the damage caused to the DNA by prolonged exposure to UV light. The agarose slice is transferred to a 1.5 ml eppendorf tube and then weighed to calculate the amount of the solutions needed for the isolation. A gel solubilization solution is added in an amount that is 3 times the weight of the gel. It is incubated for 10 minutes at 60 ℃ with the occasional gently flicking of the tube to ensure the gel is completely dissolved. This solution contains a pH indicator and yellow color represents an optimal pH. If the solution turns red, it is necessary to add 3 M sodium acetate buffer, pH 5.2, to adjust the pH to its optimum. Once the gel is dissolved, isopropanol in the same volume as the weight of the gel is added to the tube. The isopropanol is used to precipitate the DNA from the solution so that the salts and dyes can be washed away in the next steps. During the solubilization steps, the silica membrane of the spin column must be activated with a Column Preparation Solution. A spin column is inserted into a provided 2 ml collection tube. Then 500 µl of the solution is added and the column is centrifuged at 12,000 xg for 1 minute. The flow-through liquid is then discarded. 700 µl of the solubilized gel is now transferred to the activated binding column and centrifuged at 12,000 xg for 1 minute to bind the DNA to the membrane. The flow-through liquid is then discarded. If the solubilized gel had a volume greater than 700 µl, the remaining volume is again applied to the column and spun. With the DNA bound to the membrane, the column is washed with 700 µl of the Wash Solution to remove all contaminants. After a centrifugation at 12,000 xg for 1 minute, the flow-through liquid is again discarded. The column is centrifuged again for an additional 3 minutes at 12,000 xg to remove any ethanol traces that will inhibit downstream enzymatic processes. The column is then placed in a new 2 ml collection tube and the DNA elution step begins by adding to the centre of the membrane 50 µl of the Elution Solution prewarmed to 65 °C. After 1 minute incubation at room temperature, the column is centrifuged at 12,000 xg for 1 minute. The eluted DNA is now in the flow-through eluate. The DNA concentration is then measured using the NanoDrop 1000 Spectrophotometer (Thermo Scientific). The DNA sample is ready for use or stored at -20 °C.

3.2.5. Restriction digests

The digestion of our amplicon and the target expression plasmid with the same restriction endonucleases will produce complementary overhangs that will join the two molecules. A restriction digest consists of all components listed in Table 5. The final reaction volume is determined by the amount of DNA that needs to be processed. The more DNA, the more restriction enzyme required. In order to retain the enzymatic activity for long periods of time, the restriction enzymes are stored at -20 ℃ in 50% glycerol. This eliminates any water turning into ice that can damage the proteins. However, the enzyme is only active when the total glycerol content is less than 4-5%. With this in mind, the total reaction volume should not be too large, as we do not want to dilute the DNA so much that it has limited contact with the restriction enzymes. Therefore, in the sample indicated below, 1 µg DNA is placed in a reaction volume of 20 µl, which results in just 2.5% glycerol. The volume of DNA is calculated based on its concentration. Once the volumes of all other components are determined, the remaining volume is filled with MilliQ water. The reaction mixture is mixed well in a 1.5 ml eppendorf tube and briefly spun down at low speed to gather all the reagents at the bottom of the tube. Finally, since the restriction enzymes are fast digesting, the digestion is incubated in a 37 ℃ heating block for just 15 minutes. When larger amounts of DNA need to be processed, the reaction volumes, amount of enzymes and the incubation time will increase.

Table 5: Restriction digest reaction setup.

Component	Volume
DNA (1 µg)	X µl
10x Buffer	2 µl
Restriction Enzyme I	0,5 µl
Restriction Enzyme II	0,5 µl
MilliQ	Y µl
TOTAL VOLUME	20 µl

3.2.6. Ligation

Digesting two DNA molecules with the same restriction enzyme creates two complementary single-stranded overhangs that can anneal with each other. The 5'-phosphoryl and 3'-hydroxyl ends are then covalently sealed together by a T4 DNA ligase that generates a phosphodiester bond (https://www.khanacademy.org). The most commonly used ligase originates from the bacteriophage T4 that infects *Escherichia coli bacteria* (https://www.worthington-biochem.com).

The ligation reaction consists of the reagents listed in Table 6. First, the molarity of the DNA molecules (the linearized plasmid and the amplicon insert) are calculated using formula 1, where c is the DNA concentration and n is the number of nucleotides in the molecule. The constant 0.325 is the average molecular weight of all four nucleotides.

$$M = \frac{c}{0.325 \times n} \quad (1)$$

In order to promote the insertion of the amplicon into the much larger linearized plasmid, a 3:1 molarity ratio of insert to vector is calculated. Due to the probability of ligating the correct molecules together, the goal is to have between 50 and 200 ng of total DNA. Since the molarity of the larger plasmid will be much greater than the smaller amplicon, the amount of linearized plasmid is typically 1 µl if the concentration permits. The amount of the amplicon is then calculated based the amount of plasmid used. Finally, MilliQ is calculated to bring the total reaction volume to 10 µl. A negative control reaction is also prepared similarly, but without the amplicon. The number of bacteria transformed with this DNA will indicate how much of our linearized plasmid was contaminated with uncut plasmid. The tubes with the ligation mixture were then incubated overnight at 4 ℃.

Table 6: Ligation reaction setup.

Component	64ng DNA	Negative control
MilliQ	Y µl	7 µl
10x Ligase buffer	1 µl	1 µl
Linearized plasmid	1 µl	1 µl
Amplicon insert	X µl	-
T4 DNA ligase	1 µl	1 µl
TOTAL VOLUME	10 µl	

3.2.7. Transformation

In order to significantly amplify the amount of the successfully ligated plasmid containing our amplicon, we want to put it into bacteria where it can replicate in high numbers and the bacterial cultures can be grown to high density. The process in which bacteria take up plasmid DNA is called transformation, a naturally occurring mechanism for horizontal gene transfer. To promote transformation, the bacteria are made competent by changing the permeability of the cell membrane and the cell wall. This is typically done by chilling the bacteria in a $CaCl_2$ solution. Tubes with 60 µl of these cells are gently thawed from the -80 ℃ freezer on ice for 10 to 20 minutes. After the cells are thawed, 3 µl of the ligation reaction is added to the

competent cells and gently mixed. Mixed cells are incubated on ice for another 10 to 20 minutes. Transformation is initiated with a heat shock step that creates temporary pores in the bacterial cell membrane. Specifically, the bacteria are heated at 42 ℃ for 45 seconds and then immediately placed on ice for 2 minutes so the cells can recover. The transformed bacteria are then stimulated to grow by placing them in 250 µl of sterile SOC (super optimal catabolite suppressing broth), a rich nutrient medium containing glucose. This medium serves to rebuild the cell membrane and cell wall, while the glucose promotes growth, energy metabolism, and faster regeneration. The bacterial culture is then incubated at 37 ℃ for 45 minutes in a shaking incubator. To positively select for the growth of bacterial colonies containing the desired plasmid, 250 µl of transformed cells are seeded onto an LB agar plate containing 50 µg/ml of the antibiotic ampicillin (Table 7). Only bacteria with the plasmid can produce the beta-lactamase enzyme that can hydrolyze the lactam ring of ampicillin. The plate is then placed bottom up in an incubator at 37 ℃ overnight. By placing the plate upside-down, it avoids the risk of condensed water that would form on the lid from falling onto the bacteria. This is important because we do not want to disturb the formation of bacterial colonies that originated from a single cell, ensuring they all have the same genetics. The plates are incubated for no longer than 12 to 16 hours to prevent the secretion of the beta-lactamase from creating a halo of degraded ampicillin around the colony that will allow the growth of bacterial that do not contain the plasmid.

Table 7: Composition of the LB agar plate.

Reagent	[Stock]	Amount	[Final]
MilliQ		400 ml	
Tryptone		5 g	1%
Yeast Extract		2.5 g	0.5
NaCl	58.44 g/mol	0.25 g	8.5 mM
NaOH		adjust pH to 7.3	
MilliQ		fill up to 500 ml	
Agar		7.5 g	
TOTAL VOLUME	500 ml		

3.2.8. Colony screening by restriction digest

To determine if any of the individual bacterial colonies on the transformation plate contained the plasmid with our gene of interest, plasmid DNA was isolated from 5 ml bacterial cultures using GenElute™ Plasmid Miniprep Kit (Sigma-Aldrich). The isolated plasmid DNA

was then digested with selected restriction enzymes. The reaction was performed in a tube by adding 1 µg of plasmid DNA, the volume calculated based on the plasmid concentration. The following reagents were also added: 2 µl of 10x green buffer, 0.5 µl of restriction enzyme ApaI, 0.5 µl of restriction enzyme HindIII, and an amount of MilliQ to give a total volume of 20 µl. The reaction mixture was incubated for 15 min at 37 °C. 20 µl of each sample and 10 µl of a GeneRuler 1 kb Plus DNA Ladder (Thermo Scientific, cat. # SM1332) were loaded onto a 0.8% agarose gel with 1 µl ethidium bromide. The gel was run at 90 V for 1 hour and further analyzed on a Chemidoc to determine if bands of the expected size were present.

3.3. Western Blot

Western blot is a method that determines the size and abundance of individual proteins in complex samples using specific antibodies. This method is based on the separation of proteins depending on their size and subsequent transfer to a membrane on which appropriate antibodies are applied to mark the protein (Mahmood & Yang, 2012).

3.3.1. Whole cell lysate preparations

In order to resolve individual proteins based on their size, proteins from whole cell lysates must be isolated and denatured. To ensure the detection of probed proteins, the goal is to load whole cell lysate samples originating from $1x10^7$ total cells. Ideally, we would like to have enough of each sample to run multiple polyacrylamide gel electrophoresis (PAGE). This will allow us to multiplex and probe for multiple proteins or have extra material in case we encounter some technical problem. Therefore, we would like to harvest between $5x10^7$ and $1x10^8$ total parasites. Since they only grow to $1\text{-}2x10^6$ cells/ml, we will need to expand our cultures to 50 ml in a larger 75 cm^2 flask. On the day that the whole cell lysates will be prepared, the cell cultures will be counted to calculate the volume needed to harvest $1x10^8$ cells in a 50 ml falcon tube. After centrifuging at 1,300 xg for 10 minutes at 4 ℃, a cell pellet is formed at the bottom of the tube. The supernatant is then carefully poured out to prevent the disruption of the pellet. All the following steps are performed on ice or at 4 ℃ to limit protein degradation caused by the accidental lysis of some parasites during manipulations. The pellet is resuspended in 1 ml of 1x PBS-G, which is a phosphate buffered saline solution with 6 mM glucose. This buffer is applied to help maintain physiological pH, osmolality, and ion concentrations. The glucose provides energy to parasites during these processing events. The resuspended cells are transferred to a 1.5 ml eppendorf tube and centrifuged at 1,300 xg for 10 minutes at 4 ℃. The

supernatant is discarded and the cell pellet is resuspended in 1x PBS (phosphate buffered saline) (Table 8) and 3x SDS-PAGE loading dye. Importantly, the loading dye contains the detergent sodium dodecyl sulfate (SDS), which carries a negative charge that coats each protein. This has the effect of denaturing each protein as the negative charges of the SDS repel each other. The loading dye also has glycerol to help the sample sink into the well. Since the wells on the SDS-PAGE gels can only hold a maximum volume of 40 µl, a whole cell lysate from $1x10^7$ parasites should be 30 µl. Therefore, if $1x10^8$ parasites were harvested, the cell pellet should be resuspended in 200 µl 1x PBS and 100 µl 3x SDS-PAGE loading dye. The protein sample is further denatured by incubating at 97 °C for 8 to 10 minutes. This also helps to reduce the viscosity of the sample as all the released genomic DNA is cleaved into smaller fragments. The protein sample is then allowed to cool to room temperature before being stored at -20 °C.

Table 8: Composition of 1x PBS.

Reagent	[Stock]	Amount
NaH_2PO_4 x $12H_2O$	358.14 g/mol	17.9 g
NaH_2PO_4 x $2H_2O$	156.0114 g/mol	10.14 g
NaCl	58.4414 g/mol	85.0 g
MilliQ		fill up to 1 l
TOTAL VOLUME	1 l	

3.3.2. Gel electrophoresis

The function of electrophoresis in western blotting is to resolve a complex mixture of proteins based on their size. The electrophoresis occurs in a buffer tank with positive and negative electrodes. The tank holds two SDS-PAGE gels, which creates two chambers into which a 1x SDS running buffer is poured about halfway up the tank (Table 9). An electric field is applied to the fully submerged gels and the negatively charged proteins migrate into and through the gel towards the positively charged cathode. Commercially available Novex precast gels are used in the lab. These tris-glycine gels are created with a 4-20% polyacrylamide gradient to thoroughly resolve both small and large proteins on a single gel. Before the protein samples are loaded, each well is thoroughly cleaned by pipetting up and down to remove any possible acrylamide that would interfere with the sample entry into the gel. Samples are then loaded into the gel, 30 µl of each whole cell lysate is accompanied by a single well containing 4 µl of the PageRuler Prestained Protein Ladder that is used as a reference for relative protein mass. The gel was run at 90 V for 20 min until the samples completely entered the gel. Then the voltage is increased to 110 V and the gel is allowed to run for 1 to 2 hours as needed. Since

the leading edge dye of the protein samples can interfere with the subsequent probing step, the voltage is applied until this bromophenol blue dye is run out of the gel.

Table 9: Composition of 10x SDS running buffer. For 1x SDS running buffer, this buffer was diluted 1:10 with MilliQ.

Reagent	[Stock]	Amount	[Final]
Tris	121.14 g/mol	30.3 g	0.25 M
Glycine	75.07 g/mol	144.4 g	1.9 M
SDS	288.37 g/mol	10 g	1%
MilliQ		fill up to 1 l	
TOTAL VOLUME		1 l	

3.3.3. Protein transfer

Due to the fragile nature of the protein gels, the resolved proteins are transferred from the gel to a PVDF (polyvinylidene difluoride) membrane before they are probed with antibodies. First, all the components need to be prepared for blotting. The gel is carefully removed from the plastic housing, and the bottom end is cut off with a razor blade. The gel is then equilibrated in chilled 1x Transfer buffer, which offers a medium suitable for protein transfer and promotes the efficiency of protein binding to the membrane (Table 10). After the PVDF membrane is cut to the size of the SDS-PAGE gel (8.5 x 9 cm), it is activated in methanol for 40 seconds. It is then washed for 2 minutes in MilliQ water before it is equilibrated in the 1x Transfer buffer for at least 5 minutes.

Table 10: Composition of 10x transfer buffer.

Reagent	[Stock]	Amount	[Final]
Glycine	75.07 g/mol	29.3 g	390 mM
Tris	121.14 g/mol	58.15 g	480 mM
MilliQ		fill up to 1 l	
TOTAL VOLUME		1 l	

A blot sandwich is created to provide support and conductivity between the SDS-PAGE gel and PVDF membrane. The sandwich has a plastic support grid on either end, the black grid will be orientated closest to the negative anode, while the red grid will be placed close to the positive cathode. Immediately inside of each plastic grid is a blue sponge followed by a piece of whatman paper. Finally, in the middle of the sandwich is the SDS-PAGE gel, orientated towards the black grid, and the PVDF membrane facing towards the red grid. A plastic roller is

used to gently press out any air bubbles between each layer. The blot sandwich is inserted into the transfer apparatus and the tank is filled to the top with chilled 1x Transfer buffer. The transfer tank is placed at 4 ℃ and then 90 V are applied for 90 minutes. After the transfer is complete, each layer is removed to isolate the membrane. The top right corner is cut to indicate which side of the membrane the proteins are on. The membrane is carefully transferred to 45 ml of 5% milk in a 50 ml conical tube. Before being stored overnight at 4 ℃, the membrane is rotated at room temperature for 1 hour to block the blot.

3.3.4. Probing with antibodies

Once the membrane is blocked, the proteins are probed with primary antibodies that bind the target protein. Primary antibodies can either be polyclonal or monoclonal. Polyclonal antibodies are isolated from the serum of an animal, usually a rabbit. These antibodies can recognize multiple epitopes within the target protein. This helps to amplify the signal in the western blot. Monoclonal antibodies are secreted from isolated immune cells fused with an immortal cancer cell. The cells can be repeatedly frozen and thawed to generate more antibody when needed. These antibodies detect just a single epitope of the target protein and they tend to originate from mice.

The appropriate primary antibody is added directly to 5 ml of 5% skim milk so that the dilution is somewhere between 1:1000 and 1:5000. The exact dilutions have been determined previously and they depend on the avidity of the antibody and the level of target protein expression. The milk is dissolved in 1x PBS-T, which is a phosphate-buffered saline containing the detergent tween (Table 11). The purpose of the tween is to prevent non-specific antibody binding. The blot is rotated in a 50 ml conical tube, containing the milk and diluted antibody, for 1 hour at room temperature. The milk with the antibody is then discarded and the membrane is washed in three steps. First, the membrane is quickly rinsed with 20 ml of 1x PBS-T to remove any traces of milk with unbound antibody. The PBS-T wash is then replaced with 20 ml of fresh 1x PBS-T and the blot is washed for 15 minutes on a rotator. The PBS-T is discarded again and the same amount of PBS-T is added as before. This time the blot is only washed for 5 minutes, but these shorter washes are repeated for a total of three washes, with fresh 1x PBS-T added each time. The same procedure is them repeated for the secondary antibody generated in goats to recognize either the mouse monoclonal or the rabbit polyclonal primary antibodies. These secondary antibodies are also conjugated with the enzyme horseradish peroxidase (HRP), which is important for the following visualization step involving chemiluminescence. The only

difference with the secondary antibody, is that less is needed. Therefore, 2.5 µl of the correct antibody is added to 5 ml of 5% skim milk for a dilution of 1:2000.

Table 11: Composition of 1x PBS-T.

Reagent	[Stock]	Amount	[Final]
MilliQ		800 ml	
10x PBS		100 ml	1x
Tween 20	1227.72 g/mol	500 µl	0.05%
TOTAL VOLUME		1 l	

3.3.5. Visualization with ECL on Chemidoc

To visualize the antibodies on the western blot using chemiluminescence, the Clarity Western ECL Substrate from BioRad is applied. The ECL reagent consists of 2 solutions, a luminol solution and a peroxide solution that are mixed in 1:1 ratio. Luminol is an HRP substrate that emits chemiluminescence when catalyzed by HRP. However, luminol only faintly emits light, so enhancers are added to the ECL to increase the signal. The membrane is removed from the conical tube and the excess liquid is removed by capillary action. The membrane is placed between two plastic sheets and 200 µl of the ECL reagent is applied to the membrane directly where the target protein is expected to migrate. The visible colored protein ladder is used as a size reference. All bubbles between the plastic sheet are removed and the membrane is incubated for 1 minute at room temperature. The chemiluminescence is then visualized by a digital imager, like the Chemidoc MP Imaging System from BioRad.

3.4. Transfection of dyskinetoplastids

Transfection is a technique that enables foreign nucleic acids to access eukaryotic cells. Once the DNA is taken up by the cell, it can affect gene expression by overexpressing the desired gene or silencing it (Chong et al., 2021).

3.4.1. Plasmid linearization:

For stable DNA transfections that help with the uniformity of gene expression manipulation, it is best to linearize the plasmid so it can be more readily integrated into the genome of the targeted organism. The Not I linearization of the expression plasmid used in this project produces a molecule with 5‘ and 3‘ ends that are complementary to the *T. brucei* rRNA spacer locus. This results in high rates of homologous recombination to insert the expression

plasmid into the genome. Our transfection protocol stipulates that 10 µg of linearized DNA be used within the parameters outlined. Therefore, 20 µg of plasmid DNA was digested, as a significant amount of DNA is lost during the precipitation step. All reagents were added to the tube to make a final volume of 60 µl or 120 µl depending on the volume of plasmid required (Table 12).

Table 12: Plasmid digest reaction.

Reagent	60ul Rxn	120ul Rxn
Plasmid (20ug)	Xul	Xul
MilliQ	49ul-X	103ul-X
10x FD buffer	6ul	12ul
NotI	5ul	5ul

The digested linearized plasmid needs to be precipitated to isolate and concentrate the DNA before it is resuspend in sterile MilliQ water. 5 µl of 3M sodium acetate, a salt to neutralize the DNA, is added to the restriction digest. Then 125 µl of 97% ethanol is added, allowing the salt to bind the DNA and precipitate it. To enhance the rate of precipitation, the DNA is incubated in the -80 °C freezer for 30 minutes. The DNA is then centrifuged at maximum speed at 4 °C for 30 minutes. The resulting DNA pellet was washed with 200 µl of 70% ethanol and centrifuged again at maximum speed at 4 °C for 30 min. Residual ethanol was removed and the tube was allowed to dry for 8 min. The pellet was then resuspended in 30 µl of sterile MilliQ water that had been preheated to 65 °C. 3 µl of the resuspended DNA was transferred to a new tube for further analysis. 2 µl of this sample were used to measure the concentration on the nanodrop and 1 µl was visualized on an agarose gel to verify that the plasmid had been linearized. A 0.8% agarose gel was prepared in 70 ml of 1x TAE and 1 µl of 5 mg/ml ethidium bromide. 10 µl of a DNA ladder was loaded onto the gel. This was followed by a sample containing 500 ng of uncut plasmid for comparison. Finally, 10 µl of the prepared linearized plasmid was loaded. This sample consisted of 1 µl of linearized DNA, 8 µl of MilliQ and 1 µl of 10x DNA loading Dye. The gel was run at 90 V for 45 min. The results were visualized and photographed on the Chemidoc.

3.4.2. Prepare Trypanosoma culture

The DK164 pSMOX and *T. evansi* pSMOX cell lines were expanded 3 days prior to transfection into a larger 150 cm^3 flask, where 2.5 ml of culture was added to a flask containing 20 ml of HMI-11 medium with 100 ng/ml of puromycin, an antibiotic to which the cells are

resistant. The cells were allowed to grow overnight. The next day, the concentration in each flask was counted and the cells were seeded at a concentration of $8x10^4$ cells/ml into a 50 ml culture. The cells were allowed to grow overnight. The timing and amount of parasites used to seed the culture are important because the transfection should be performed when the cell line is growing in mid-log phase. This ensures that they are replicating frequently and increases the opportunities for homologous recombination.

3.4.3. Transfection protocol

The following afternoon, $3x10^7$ cells were centrifuged at 1,300 xg for 10 minutes at room temperature. The cells were washed with PBS-G and spun again. The cell pellet was then resuspended in 100 µl Amaxa Cell Line Nucleofector by Lonza. Resuspended cells were transferred to a 2 mm gap electroporation cuvette and mixed with 10 µg of the linearized plasmid. Cuvettes were placed in the Nucleofector II electroporator by Lonza and program X-001 was used. After electroporation, the transfected parasites were placed in 30 ml of HMI-11 containing 100 ng/ml puromycin and mixed well by inverting the tube. 3 ml of the diluted transfectants were then transferred to a new tube already containing 27 ml of media, further diluting the cells to a concentration of $1x10^5$ cells/ml. The final step in the serial dilution was to transfer another 3ml from the previous dilution into a new tube, resulting in $1x10^4$ cells/ml. 1 ml aliquots were then distributed to a 24 well plate for each dilution and incubated at 37°C. After 16 hours, 1 ml of fresh media containing 2x the final concentration of the selective antibiotic (10 µg/ml hygromycin) was added to each well. Positively selected transformants typically became dense between 5 to 7 days after the transfection.

3.4.4. Selection process

After 5 days, 24-well plates were analyzed under a microscope to determine cell viability and concentration. Approximately 5 wells from each 24-well plate that had the best conditions and ideal concentrations were selected and plated on a new 24-well plate and divided each day according to their concentration. In order not to stress the parasites, they were sequentially diluted more aggressively, with a regimen similar to the following: 1:1, 1:2 or 1:3. Each time the parasites were split, fresh medium containing 100 ng/ml puromycin and 5 µg/ml hygromycin was added to keep the volume at 2 ml. After a week of maintaining the cells in this manner, the cells were transferred to larger 25 cm^3 flasks and the culture volume was increased to 10 ml.

3.5. DAPI staining

An immunofluorescence assay (IFA) with DAPI (4',6-diamidino-2-phenylindole) staining is a method used to visualize the nuclear and mitochondrial genomes of the parasites. First, a total of $2x10^7$ cells were harvested in a 50 ml tube and centrifuged at 1,300 xg for 10 minutes at room temperature. The media was carefully poured off to avoid disturbing the cell pellet, which was resuspended in 1 ml of 1x PBS and transferred to a 1.5 ml eppendorf. It was then centrifuged at 1,300 xg for 10 min at room temperature. The supernatant was pipetted off and the cell pellet was resuspended in 200 µl of 1x PBS. Then 200 µl of 2x formaldehyde solution was added to fix the cells.

The coverslips were coated with 20 µl of poly-L-lysine and allowed to dry for 1 hour. 40 ul of the fixed cells were added to the pre-prepared coverslips and incubated for 15 min at room temperature. Next, the coverslips were washed three times with 100 µl 1x PBS. Then the coverslips were mounted onto microscope slides using two drops of ProLong Glass Antifade Mountant with NucBlue. The coverslip was gently pressed to remove any bubbles. The parasites from these microscope slides were finally visualized under an Axioplan 2 Zeiss fluorescence microscope with an Olympus DP73 CCD camera.

3.6. Growth curves

Growth curves are used to graphically display the rate of cell growth as a function of time. They are used to analyze the doubling time between cultures treated under different conditions. In this case, for each transfected clone, we compared the growth rate of parasites induced to express ASCT to those that were not treated with tetracycline. Approximately 5 clones of each transfected cell line were allowed to grow in 25 cm^3 flasks. There were 2 flasks of each clone that would represent either the noninduced or induced cultures. The cells were counted and their concentration was recorded every 24 hours for 7 days. After measuring the cell density, both flasks were split to $2.5x10^5$ cells/ml in 5 ml of fresh HMI-11. To one flask from each clone, 1 µg/ml of tetracycine was added daily to induce protein expression by removing the Tet repressor from the Tet operon and allowing transcription to proceed. These flasks were placed in a 5% CO_2 incubator at 37 °C.

To plot the data, the values were first calculated in an Excel spreadsheet to calculate the cummulative density. The cummulative density is a value representing the concentration of the culture in a theoretically ideal flask, one so large that the cell population could double

indefinitely without reaching restrictive cell densities. Each day, the amount needed to seed the culture to $2.5x10^5$ cells/ml was calculated from that day's cell density. This volume was then subtracted from the total 5 ml culture volume to determine how much fresh HMI-11 medium was to be added. Then the daily dilution factor was calculated by taking the inverse of the seeded volume divided by 5. The cummulative dilution factor was then calculated by multiplying all the previous daily dilution values together. Finally, to express the cummulative cell density of the population in a flask, that day's cell density was multiplied by that days's cummulative dilution value. Plotting the values in this manner makes it easier to recognize changes in growth rates over longer periods of time.

3.7. Mitochondial membrane potential

Healthy mitochondria have an energized inner membrane that is essential for the protein import of nuclear encoded gene products. This mitochondrial membrane potential ($\Delta\Psi_m$) is generally the result of the active proton pumps within the electron transfer chain complexes. Using a Fluorescence-Activated Cell Sorting (FACS) machine, the amount of fluorescence can be measured from the positively charged dye, Tetramethylrhodamine ethyl ester (TMRE). The amount of TMRE that accumulates in the mitochondria is directly proportional to the strength of the $\Delta\Psi_m$ (Crowley et al., 2016). During flow cytometry, cells move one at a time across a laser beam with a 488 nm wavelength. This laser beam supplies the excitation energy that TMRE then converts into a 585 nm emission light that is detected. Carbonyl cyanide-p-trifluoromethoxyphenylhydrazone (FCCP) is an ionophore that disrupts mitochondrial oxidative phosphorylation by providing a pathway for protons to cross the inner mitochondrial membrane. The addition of FCCP should dissipate the $\Delta\Psi_m$ measured by fluorescence intensity.

3.7.1. TMRE staining

Each transfected cell culture was grown to log phase ($1x10^6$ cells/ml) in three separate flasks. Two of the flasks were treated with 1 μg/ml tetracycline to induce the expression of ASCT for either one or two days. The third flask was not treated with tetracycline and was used as a reference. Each cell culture was counted and $5x10^6$ cells were harvested at 1,300 xg for 10 minutes at room temperature. The media was decanted and the cell pellet was resuspended in 1 ml of HMI-11 containing 60 nM TMRE. For the negative control, the cell pellet was resuspended in 1 ml of HMI-11 containing 60 nM TMRE and 20 μM FCCP. The samples were incubated at 37°C for 30 min. After incubation, 1 ml of 1x PBS (pH 7.4) was added to each tube and 200 μl were transferred from these tubes to prepared FACS tubes.

3.7.2. Fluorescence measurements on FACS

Cell samples in FACS tubes were analyzed with a Becton Dickinson FACS Canto II flow cytometer to measure the fluorescence emitted by TMRE. Additionally, each cell's size (forward scatter = FSC) and granularity (side scatter = SSC) were recorded. Microsoft Excel was used to extract data from the FACS computer and further analyses were performed.

4. Results

4.1. Expression levels of enzymes required for the mitochondrial substrate phosphorylation

In the mitochondrion of *T. brucei*, SCoAS can directly generate ATP via substrate phosphorylation as it converts succinyl-CoA to succinate. To determine if there might be different levels of substrate phosphorylation between trypanosomes with and without mitochondrial DNA, we first compared SCoAS expression levels between BF *T. brucei* wt, the parental lab-induced and natural dyskinetoplastids (DK164 and *T. evansi*, respectively) and the dyskinetoplastids genetically modified for inducible protein expression (DK164 pSMOX and *T. evansi* pSMOX*)*. Therefore, western blots comprised of whole cell lysates resolved by polyacrylamide gel electrophoresis were probed with polyclonal antibodies generated against SCoAS. The enzyme levels were then detected by chemiluminescence on the Chemidoc MP. While SCoAS was detected in all samples, the levels of expression varied between the cell types (Figure 6). The amount of enzyme was decreased in both DK164 cell lines compared to BF *T. brucei* wt. The SCoAS expression level was even further repressed in the *T. evansi* cell lines. Due to the equal amounts of mtHSP70 observed in each sample, these differences in SCoAS levels are not the result of sample manipulation or uneven loading. Instead, they indicate that trypanosomes lacking mitochondrial DNA modify the total amount of an enzyme directly involved in mitochondrial substrate phosphorylation.

In *T. brucei*, mitochondrial substrate phosphorylation can also occur through the ASCT/SCoAS cycle, which is essential for acetate production in the BF wt parasites. To understand the robustness of this system, the same samples were probed with polyclonal antibodies raised against ASCT. Again, the same pattern of enzyme expression was detected between the cell lines as observed for SCoAS. The ASCT expression in the lab generated strain DK164 is lower than in BF *T. brucei* wt, but still more abundant compared to the naturally occurring dyskinetoplastic strain of *T. evansi* where ASCT is hardly detectable (Figure 6).

Since the two main enzymes involved in the generation of mitochondrial ATP by substrate phosphorylation are significantly repressed in parasites lacking mitochondrial DNA, we also wanted access the steady state levels of other bioenergetic components. The abundance of the mitochondrial ATP/ADP carrier, AAC, was largely unchanged between the BF *T. brucei* wt and DK164 cell lines.

However, AAC does appear to be lower in *T. evansi*, suggesting that AAC expression levels are modified in conjunction with significantly depleted substrate phosphorylation capabilites. Conversely, the expression of the ATP synthase subunit beta is slightly reduced in both DK164 and *T. evansi* compared to BF *T. brucei* wt parasites.

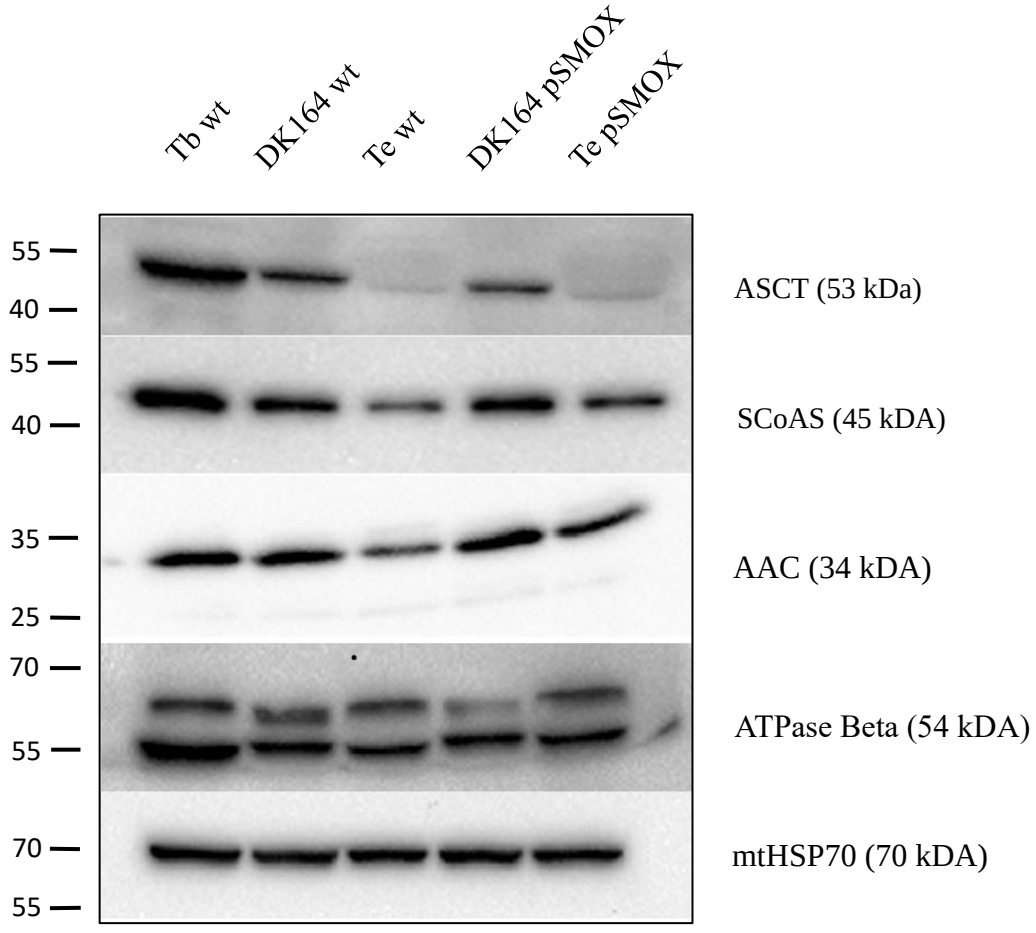

Figure 6: Bioenergetic protein levels in various dyskinetoplastic strains determined by immunoblotting. Whole cell lysates were prepared from the following cell lines: BF *T. brucei* wt (Tb wt), DK164 wt, DK164 pSMOX, *T. evansi* wt (Te wt) and *T. evansi* pSMOX (Te pSMOX). The equivalent of $1x10^7$ cells were loaded for each sample onto a Novex 4-20% Tris-Glycine Mini polyacrylamide gel. Resolved proteins were transferred to a PVDF membrane and then immunoblotted with the following primary antibodies and their dilutions:

Acetate:succinate CoA transferase (ASCT) – 1:1000; succinyl-CoA synthetase (ScoAS) – 1:1000; ADP/ATP carrier (AAC) – 1:1000; ATP synthase subunit beta (ATPase Beta) – 1:5000; mitochondrial heat shock protein 70 (mtHSP70) – 1:5000. Chemiluminescence was visualized on the Chemidoc MP Imaging system (BioRad). Sizes in kDa of the relevant protein ladder are indicated to the left of the blot, while the expected size of the detected proteins are indicated to the right.

4.2. ASCT protein alignment of *T. brucei* and *T. evansi*

The differences in the protein expression levels of various bioenergetic components between the chemically induced lab strain DK164 and the naturally occurring *T. evansi* strain are interesting, especially since both lineages are dyskinetoplastids. While the presence of an enzyme does not necessarily mean that the metabolic pathway is active, we wanted to analyse the dyskinetoplastic protein sequences to determine if there were any significant mutations in either of the proteins potentially involved in mitochondrial substrate phosphorylation. Unfortunately, we do not have sequencing data for the DK164 parasites. Since this lab strain was generated from repeated exposures to the carcinogen acriflavine, it is possible that either ASCT or SCoAS accumulated mutations that render it in active. To verify this scenario, we would need to clone and sequence these DK164 genes. While a plausible experiment, this was not an aim within the limited time frame of the thesis. However, we were able to compare the protein sequences from the reference *T. brucei* 927 strain and *T. evansi* to identify any possible changes in their composition. Sequences were obtained from the TriTryp GeneDb website (https://tritrypdb.org/tritrypdb/app/) with the following gene identification numbers for the *T. brucei* 927 strain and *T. evansi* strains respectively (SCoAS: Tb927.10.7410 and TevSTIB805.10.7880; ASCT: Tb927.11.2690 and TevSTIB805.11_01.2760). These protein sequences were then aligned using the Geneious algorithm within the Geneious software suite (version 11.1.5). Although no changes in the primary amino acid sequences of ScoAS from *T. brucei* or *T. evansi* were identified (data not shown), there were two substitutions identified within the *T. evansi* ASCT protein (Figure 7). The Geneious alignments, as indicated by the green consensus identity bar, indicate that both, 493 amino acid proteins, are identical in their sequence except for two residues, serine S419N and threonine T49. Neither of these mutations are located within the defined substrate-binding domain or catalytic active site of ASCT. While S419N is a conserved amino acid substitution with both serine and asparagine containing polar neutral side chains, the T493A substitution is not conserved as threonine has a polar neutral side chain and alanine has a hydrophobic side chain. While neither of these point mutations are

likely to render the enzyme inactive, it is interesting to note that both *T. evansi* substitutions eliminate amino acids that could potentially be post-translationally modified by phosphorylation events. However, due to the rather large number of conserved serines (18) and threonines (34) in these two protein sequences, it makes it fairly unlikely that the S419N and T493A substitutions would have a significant effect on any possible regulation of the enzymatic activity.

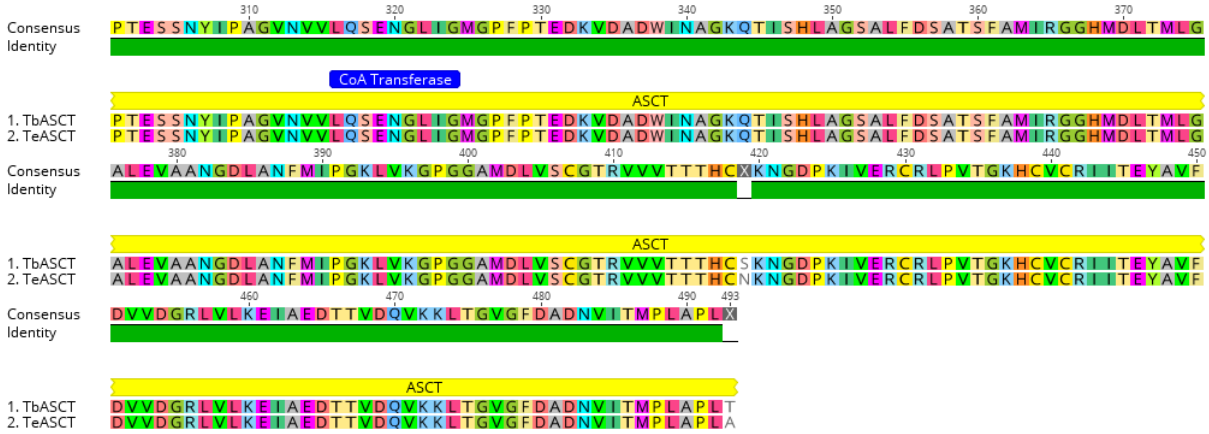

Figure 7: A representative section of the *T. brucei* and *T. evansi* ASCT protein alignments generated by the software platform Geneious. The consensus identity is presented as a solid green bar when the aligned amino acids are exactly the same. Important domains are annotated in blue bars and the numbers above the sequence indicate the amino acid position, with 1 being the start methionine.

4.3. Cloning ASCT into a protein expression plasmid

The aim of cloning is to amplify the ASCT gene from *T. brucei* genomic DNA and insert it into the expression plasmid pT7-3V5. When linearized, this plasmid is designed to be integrated into the genome of the dyskinetoplastic DK164 pSMOX or *T. evansi* pSMOX cell lines that are genetically modified for heterologous protein expression.

4.3.1. ASCT PCR amplification

Using the primer pair AZ1506 and AZ1507, the ASCT coding sequence was PCR amplified from 200 ng of isolated *T. brucei* genomic DNA. The forward primer AZ1506 contains a HindIII restriction site, while AZ1507 contains a BglII site because of an internal BamHI site in the ASCT coding sequence (Table 13). The proofreading KOD Hot Start DNA Polymerase with a 3' → 5' exonuclease was used to ensure the fidelity of the amplified DNA. 35 PCR cycles were performed on the BioRad T100 Thermal Cycler using the parameters

suggested by the polymerase manufacturer and an annealing temperature of 52 ℃. The resulting amplicon DNA was resolved on a 0.8% agarose gel stained with 0.5 µg/ml ethidium bromide. DNA fragments were visualized on the BioRad chemidoc using a UV light source. The PCR amplified a significant amount of DNA at the expected size of 1499 kb (Figure 8), which was gel extracted and digested with restriction enzymes HindIII and BglII.

Table 13: Primers used in thesis.

Primer	Nt	Sequence	Restriction Site
AZ1506	30	CGGC*AAGCTT*ATGCTCCGCCGAACAAATTT	Hind III
AZ1507	38	TAAT*AGATCT*CGTGAGGGGCGCCAATGGCATCGTTATC	Bgl II
AZ0468	20	CTGTGCCATCAGATTACTCC	N/A
AZ0500	28	AAACTTATTTTATGGCAGCAACGAGACC	N/A
T7 promoter	20	TAATACGACTCACTATAGGG	N/A

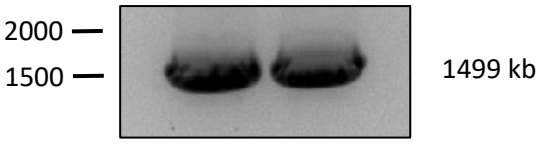

Figure 8: ASCT PCR products resolved on an ethidium bromide stained agarose gel. Relevant DNA markers in kb are indicated on the left, while the expected size of the ASCT amplicon is indicated on the right.

4.3.2. Restriction digest of the pT7-3V5 plasmid

To create complementary sticky ends to the processed amplicon, the parental expression vector was digested with the restriction enzymes HindIII and BamHI. The digested plasmid appeared as a linear molecule that migrated at the expected size (7807 kb) after being resolved on an ethidium bromide stained agarose gel. Importantly, the digested plasmid had a different profile than the uncut plasmid, which contained multiple bands representing the super coiled and nicked conformation of the circular plasmid (Figure 9). The linearized plasmid was then gel extracted and ligated with the digested ASCT amplicon to create the desired plasmid ASCT-pT7-3V5.

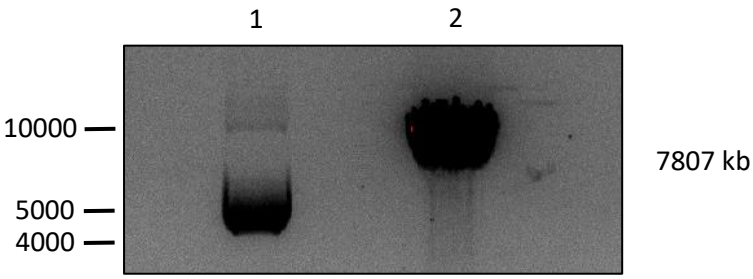

Figure 9: HindIII and BamHI restriction digest of the over-expression plasmid pT7-3V5. About 1 μg of uncut plasmid (lane 1) and all of the linearized plasmid (lane 2) was resolved on 0.8% agarose gel stained with 0.5 μg/ml ethidium bromide. Relevant DNA markers in kb are indicated on the left, while the expected size of the amplicon is indicated on the right.

4.3.3. Colony screening of ASCT-pT7-3V5 plasmid

After ligation, the ASCT-pT7-3V5 plasmid was transformed by heat shock into XL1 blue chemically competent bacteria. Transformed bacteria containing the ASCT-pT7-3V5 plasmid were selected on an LB agar plate containing 100 mg/ml ampicillin. After 16 hours of growth at 37 ℃, dozens of colonies were visible on the plate. That evening, four individual colonies were chosen and grown in nutrient-rich lysogeny broth (LB) for 16 hours. The next day, plasmids were isolated from the bacterial cultures and digested with the restriction enzymes ApaI and HindIII. The DNA fragments were analyzed on a 0.8% agarose gel (Figure 10). Using the Geneious software, the digested plasmid was predicted to result in three DNA bands of 5021, 1500 and 1300 kb. Our results indicate that the transformation was successful, as each of the bacterial colonies tested had a plasmid containing an inserted DNA fragment of the expected amplicon size.

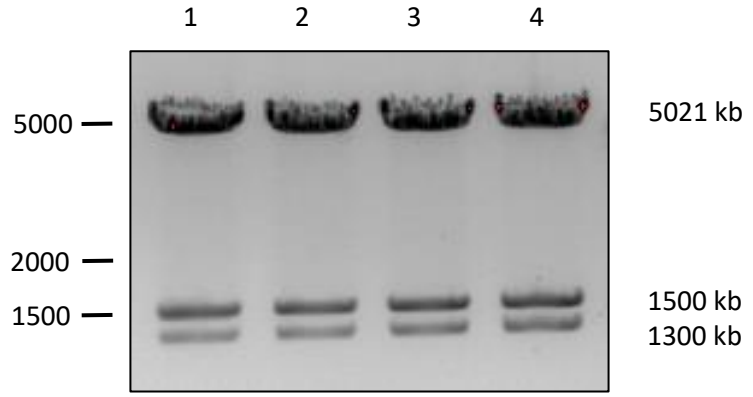

Figure 10: Plasmid restriction digests to screen bacterial colonies transformed with ASCT-pT7-3V5. 1 μg of isolated plasmids from bacterial colonies 1-4 were digested with ApaI and HindIII restriction enzymes. DNA was resolved on a 0.8% agarose gel stained with 0.5

µg/ml ethidium bromide. DNA fragments were visualized on the BioRad chemidoc using a UV light source. Relevant DNA markers in kb are indicated on the left, while the expected sizes of the DNA fragments are indicated on the right.

4.4.Sequencing of ASCT-pT7-3V5

To confirm that the ASCT gene was indeed integrated into the pT7-3V5 plasmid without any replication errors in the coding sequence, an ASCT-pT7-3V5 plasmid from a single bacterial clone was sent to the company SEQme for sequencing. SEQme generally provides about 900 bp of good sequencing data from a single sequencing reaction initiated by a provided primer. Therefore, to cover the entire 1,500 nucleotide ASCT coding sequence, we needed to sequence the plasmid with a forward (T7), reverse (AZ0500) and internal (AZ0468) primer. The resulting SEQme chromatograms were uploaded into the Geneious software and aligned with the *in silico* generated plasmids. These pairwise alignments included a green bar that indicated when the aligned nucleotides were identical. When a nucleotide discrepancy was identified by the lack of a green bar, the imported chromatograms were immediately consulted to determine if the sequencing software misidentified the fluorescent peak or if it could be omitted due to a region of poor sequencing. Each confirmed nucleotide substitution was then mapped to its location within a codon by referencing the overlaid translation sequence. These changes were recorded and special attention was paid to mutations that resulted in amino acids with different physical properties. In total, only three substitutions were identified and they all occurred at the third position of the codon (wobble position), which did not lead to a change in the encoded amino acid (Figure 11). Since these ASCT coding sequence differences were relegated to the wobble position, most likely they represent minor strain differences between the *T. brucei* 427 strain used in the lab and the sequencing reference strain *T. brucei* 927.

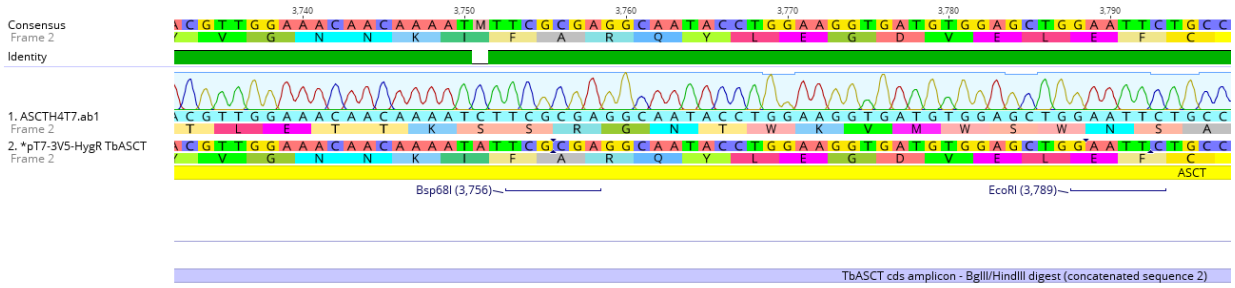

Figure 11: ASCT-pT7-3V5 sequencing colour chromatograms aligned with *in silico* plasmid. Each of the four nucleotides are represented as a coloured peak, with the height indicating the fluorescence intensity. The ASCT coding sequence is also translated in the

correct reading frame and the corresponding amino acids are coloured coded. The consensus identity, represented as a solid green bar when the aligned nucleotides are identical, quickly identifies when there is a nucleotide change between sequences. DNA alignments were performed using the software platform Geneious.

4.5.DAPI verification of dyskinetoplastic cell lines

Before any transfections were performed, we wanted to verify that the dyskinetoplastic cell lines were truly lacking mitochondrial DNA. Previously in the lab, a dyskinetoplastic cell line became cross-contaminated with BF *T. brucei* wt parasites being grown and split simultaneously. Since the dyskinetoplastic cell lines have a slower doubling time, it only takes a few days before a couple of wt parasites can outcompete the whole dyskinetoplastic culture. Since dyskinetoplastids are almost morphologically identical to BF *T. brucei* wt parasites, it is hard to distinguish the two cell lines under an inverted light microscope. Therefore, each of the cell lines were incubated with the fluorescent dye DAPI that stains both nuclear and mitochondrial DNA. When visualized under a fluorescent microscope, BF *T. brucei* wt produce a large blue fluorescent spot representing the nucleus and another much smaller fluorescent spot at the kinetoplastid DNA (Figure 12A). In contrast, the dyskinetoplastic cell lines without any mitochondrial DNA should only have fluorescence at the nucleus. Initial analyses showed that kinetoplast DNA was indeed detected in some of the supposedly dyskinetoplastic cell lines (Figure 12B). Following this finding, new dyskinetoplastic cell lines were thawed from the liquid nitrogen stabilates and confirmed that they indeed lacked mitochondrial DNA, as shown in Figure 12 (C-F).

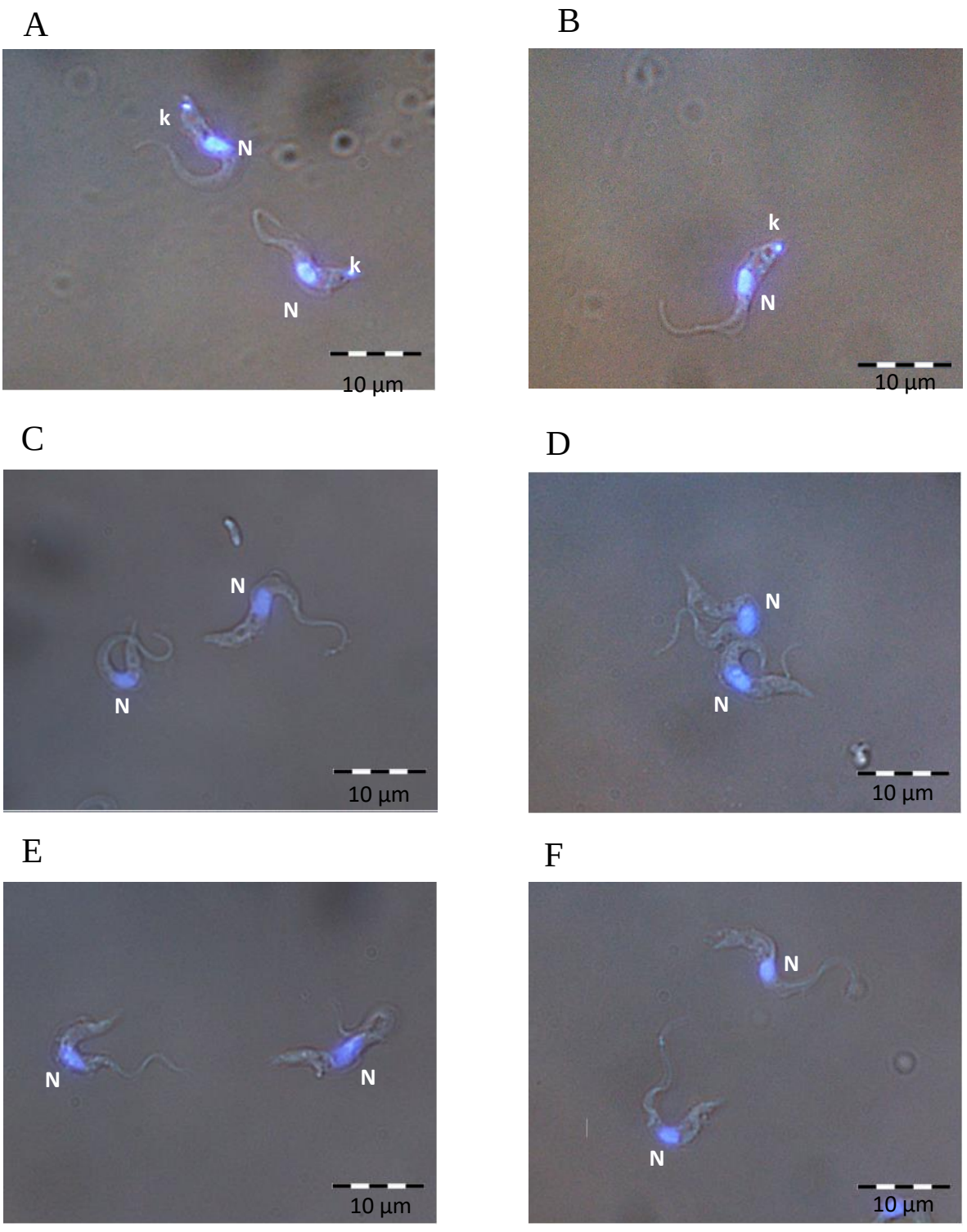

Figure 12: Fluorescent microscopy and DAPI staining were used to verify the dyskinetoplastic cell lines A) *T. brucei wt,* B) DK164 *wt* contaminated with BF *T. brucei* wt, C) DK164 *wt,* D) DK164 *pSMOX,* E) *T. evansi wt* and F) *T. evansi pSMOX.* $5x10^7$ cells fixed with 7.4 % formaldehyde were applied to glass cover slips coated in poly-L-Lysine. Cover slips were mounted on slides with ProLong Glass Antifade Mountant with NucBlue. The blue stained DNA of the nucleus (N) and the mitochondrial kinetoplastid DNA (k) were visualized

with the 100x objective of the Olympus DP73 CCD fluorescent microscope. The fluorescence images were overlayed with the Differential Interference Contrast (DIC) images. The size of the parasites can be determined from the scale bars in the bottom right corner.

4.6. DK164 pSMOX and *T. evansi* pSMOX ASCT-pT7-3V5 transfections

In order for the ASCT pT7-3V5 plasmid to efficiently integrate into the parasite genome by homologous recombination, it needs to be digested by the NotI restriction enzyme to produce a linearized molecule with 5' and 3' ends that are identical to the ribosomal DNA spacer region. Therefore, 20 µg of the plasmid was digested, precipitated and resuspended in sterile water. To verify complete linearization of the plasmid, 1 µg was analyzed on a 0.8% agarose gel alongside uncut plasmid (Figure 13). While the digested plasmid migrated around the expected size of 7,800 bp, the uncut vector was represented by the typical three conformations that circular DNA can undertake: supercoiled, relaxed and nicked.

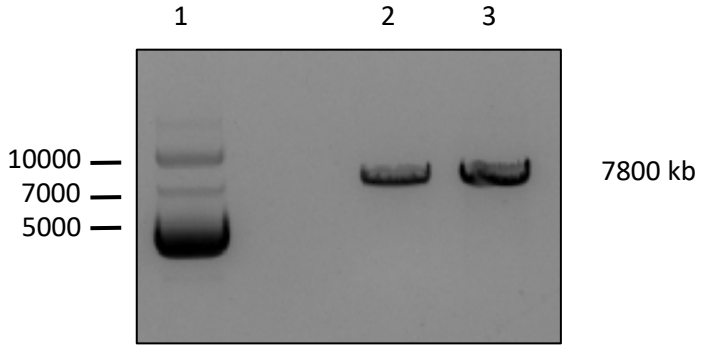

Figure 13: Linearization of the ASCT-pT7-3V5 plasmid using the fast digest restriction enzyme NotI. 1 µg of uncut plasmid (lane 1) and all of the linearized plasmid (lane 2 and 3) was resolved on 0.8% agarose gel stained with 0.5 µg/ml ethidium bromide. Relevant DNA markers in kb are indicated on the left, while the expected size of the amplicon is indicated on the right.

The DK164 pSMOX and *T. evansi* pSMOX cells lines were then electroporated with the linearized ASCT pT7-3V5 plasmid. In order to select near clonal cell lines, the transfected cells were serially diluted 1:10 before being seeded into three plates with cell densities ranging from $1x10^6$ cells/ml (Plate A) to $1x10^4$ cells/ml (Plate C). After ~5-7 days, each transfection produced wells of healthy, motile parasites. In order to avoid a mixed genetic population of transfected parasites, it is ideal to select wells from plate C, where there is the best chance that the population originated from just a few cells. However, the total number of viable clonal cell lines

was limited and for DK164 pSMOX ASCT pT7-3v5-Hyg, the following wells were selected: 1 well from Plate A, 3 wells from Plate B and 2 wells from Plate C. The success rate for transfected *T. evansi* ASCT pT7-3v5-Hyg was similar and resulted in the selection of 1 well from plate A, 2 wells from plate B and 1 well from plate C.

4.7. Growth curves of ASCT dyskinetoplastic cell lines

To test our hypothesis that the expression of an enzyme participating in mitochondrial substrate phosphorylation would have a negative effect on the health of dyskinetoplastic parasites, the growth rate was measured upon induced ASCT expression and compared to cell populations with uninduced expression. When the DK164 pSMOX ASCT-pT7-3V5 cell line was induced by tetracycline, the growth rate was significantly reduced but it was not lethal to the parasites (Figure 14A). Expression of ASCT in the naturally ocurring dyskinetoplastic *T. evansi* ASCT-pT7-3V5 cell line led to a different result. Each clone of *T. evansi* showed a cytostatic growth phenotype that proved nearly lethal within 48 hours of ASCT induction (Figure 14B). However, a population of the cells in the culture found a way to escape ASCT expression in the following days. This presumably occurred through mutations that affected the heterologous expression of the ASCT protein, allowing these parasites with a near normal rate of growth to overwhelm the culture. Unfortunately, when the *T. evansi* ASCT-pT7-3V5 cell line was re-induced for subsequent assays, the population no longer showed a growth phenotype. The same was true for the stabilates thawed from liquid nitrogen. This loss of phenotype has been observed previously in the lab when genetically modified parasites experience such a rapid and severe growth phenotype. Although we were unable to re-establish induced ASCT expression in the cells, their initial growth phenotype supports our hypothesis.

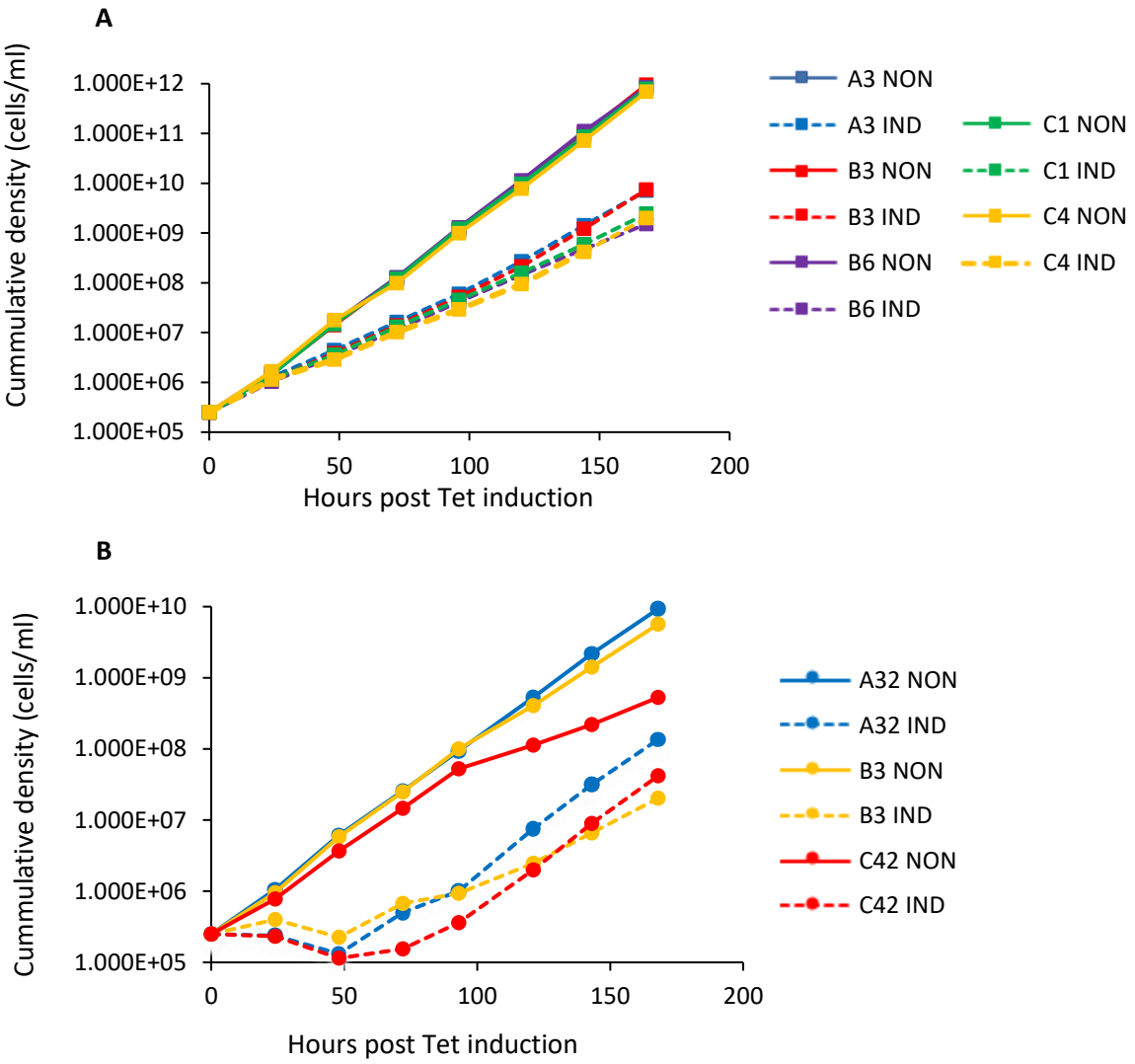

Figure 14: Growth phenotypes induced by heterologous expression of ASCT in *T. brucei* DK164 *pSMOX* (A) and *T. evansi* pSMOX (B). Each clone was grown in two separate flasks, one was induced daily with 1 µg/ml tetracycline (IND) and the other was untreated (NON). The cell density of each 10 ml culture was counted daily for 7 days. To maintain logarithmic growth, the cultures were split to $2.5x10^5$ cells/ml every day. The daily dilution factors were used to calculate the cummulative density of the cultures.

4.8. Verification of ASCT-3V5 expression in *T. brucei* DK164 pSMOX by immunoblotting

To verify that the growth phenotype correlates with ASCT expression in the DK164 pSMOX ASCT-pT7-3V5 clone C4 cell line, V5 tagged ASCT protein expression was analyzed by immunoblotting. Whole cell lysates were generated from $1x10^7$ noninduced (NON) cells and from cells treated with tetracycline for 1 (IND1) and 2 (IND2) days. The resolved proteins

were transferred to a PVDF membrane and probed with V5 tag and adenine phosphoribosyltransferase (APRT) antibodies (Figure 15). Serving as a loading control, APRT was expressed almost equally in each sample. The noninduced DK164 cells have a very faint band detected around 60 kDa by the V5 tag antibody. While these results need to be repeated, this minor ASCT expression could be the result of spill-over from the neighboring sample or it could indicate some leaky ASCT expression in parasites not treated with tetracycline. In contrast, the cell lines induced with tetracycline for 1 and 2 days expressed significant levels of V5 tagged ASCT after just 24 hours of induction. Considering that the ASCT-pT7-3V5 DK164 pSMOX growth phenotype manifested within 24 hours of tetracycline induction, it appears that growth phenotype correlates nicely with the induced V5 tagged ASCT expression.

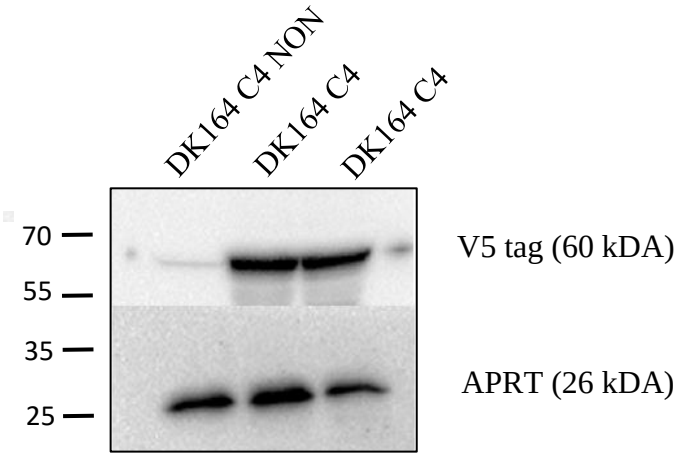

Figure 15: Inducible ASCT-3V5 tagged expression in the *T. brucei* DK164 pSMOX clone 4 cell line was verified by immunoblotting. Whole cell lysates were prepared from the following samples: *T. brucei* DK164 pSMOX clone 2 noninduced (NON) cells, as well as cells induced with tetracycline for 1 day (IND1) *or* 2 days (IND2). The equivalent of $1x10^7$ cells were loaded for each sample onto a Novex 4-20% Tris-Glycine Mini polyacrylamide gel. Resolved proteins were transferred to a PVDF membrane and then immunoblotted with the following primary antibodies and their dilutions: V5 tag – 1:2000; adenine phosphoribosyltransferase (APRT) – 1:500. Chemiluminescence was visualized on the Chemidoc MP Imaging system (BioRad). Sizes in kDA of the relevant protein ladder are indicated to the left of the blot, while the expected size of the detected protein are indicated to the right.

4.9. Measuring DK164 pSMOX ASCT-pT7-3V5 ΔΨm with TMRE

We hypothesized that increased levels of mitochondrial substrate phosphorylation would be detrimental for dyskinetoplastic parasites because as the amount of mitochondrial ATP increases, it would be more difficult for AAC to exchange cytosolic ATP^{4-} for mitochondrial ADP^{3-} generated by the F_1-ATP synthase enzyme. This would disrupt the electrogenic mitochondrial membrane potential, which is essential for mitochondrial protein import. To test this hypothesis, the mitochondrial membrane potential of DK164 pSMOX ASCT-pT7-3V5 was measured in both noninduced cells and cells induced with tetracycline for 1 and 2 days. As a reference point, the mitochondrial membrane potential of the parental DK164 wt cell line was also measured and set to 100%. Cells were stained with 60nM TMRE, a fluorescent dye that accumulates in energized mitochondria depending on the intensity of the membrane potential. The amount of fluorescence in these cell lines was measured on a FACS flow cytometer. The values obtained from the measurements were then plotted against the parental cell line DK164 wt (Figure 16). When ASCT expression is induced in the DK164 cell line, a sustained decrease in mitochondrial membrane potential occurs. This reduced mitochondrial membrane potential correlates nicely with the observed growth phenotypes. Surprisingly, the membrane potential is already significantly reduced in noninduced cells compared to the parental DK164 wt cell line. This may be due to the leaky expression of ASCT detected by immunoblotting in the noninduced DK164 cell line. Finally, treating the DK164 wt cells with the 20 μM ionophore carbonyl cyanide-p-trifluoromethoxyphenylhydrazone (FCCP) should depolarize the mitochondrial inner membrane and act as a negative control.

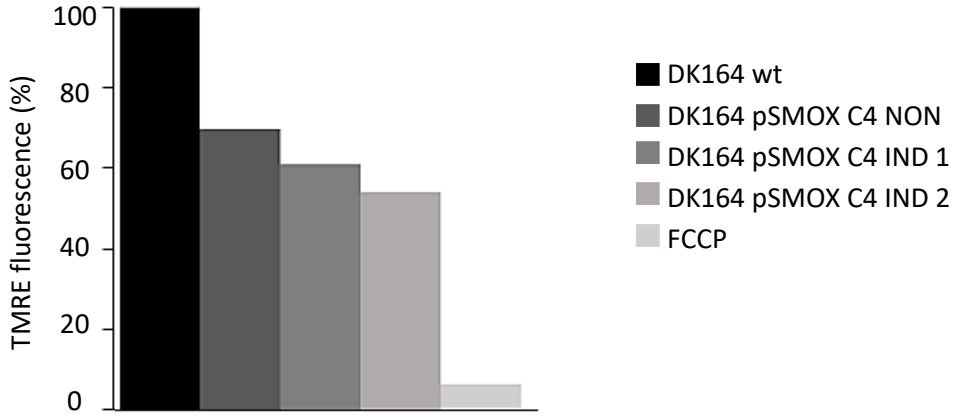

Figure 16: DK164 ASCT V5 mitochondrial membrane potentials measured by TMRE staining and flow cytometry. ASCT V5 tagged expression was either noninduced (NON) or

induced with 1 μg/ml tetracycline for one (IND1) or two days (IND2). $5x10^6$ cells were incubated with 60 nM TMRE for 30 minutes at 37 °C. Fluorescence from 10,000 events was measured on the FACS Canto II flow cytometer. The relative amount of fluorescence from each of the DK164 pSMOX cell lines was compared to that of the parental DK164 wt cell line, which was set to 100%. DK164 wt cells were treated with 20 μM of FCCP for 30 minutes.

5. Discussion

Dyskinetoplastids rely on AAC to import cytosolic ATP to maintain the essential mitochondrial membrane potential. Therefore, it is presumed that the level of mitochondrial substrate phosphorylation must be kept in check so that the mitochondrial pool of ATP does not inhibit the reverse activity of AAC. Due to the observation that BF *T. brucei* wt parasites secrete excess acetate and succinate, it is generally assumed that *T. brucei* mitochondrial substrate phosphorylation can occur in two different ways. One metabolic pathway involves SCoAS, as glutamine uptake feeds into the TCA cycle and leads to the secretion of succinate (Johnston et al., 2019). Since succinate can also be catabolized from glucose without generating ATP in the mitochondria (Figure 4), it is important to note that a portion of the excreted succinate does not contain carbon from radiolabeled glucose and must have originated from another source, possibly from glutamine. ATP can also be created from the ASCT/SCoAS cycle activated during the synthesis of acetate produced from either threonine or pyruvate (Mazet et al., 2013). Importantly, acetate production from acetyl-CoA can occur with or without ATP generation, either by the ASCT/SCoAS cycle or ACH, respectively (Figure 4). However, unpublished data from the Zíková lab indicates that BF *T. brucei* lacking ScoAS does not secrete any excess acetate. This indicates that at least some of the acetate produced will involve substrate phosphorylation and the production of ATP. While it has been proposed that BF *T. brucei* mitochondria likely generate their own pool of ATP (Mochizuki et al, 2020), unfortunately no data on the metabolism of dyskinetoplastids has been published to date.

If dyskinetoplastids need to limit the amount of mitochondrial ATP created by substrate phosphorylation, perhaps the abundance or activity of the enzymes involved in this process might be restricted. Indeed, the western blot analyses indicated that the expression levels of SCoAS and ASCT were reduced in the dyskinetoplastic parasites compared to the BF *T. brucei* wt cells. Notably, the suppression of these proteins was more dramatic in the naturally occurring *T. evansi* dyskinetoplastic strain. This discrepancy between the artificially generated lab dyskinetoplastic strain DK164 and *T. evansi* is intriguing. Since the DK164 cell line was

generated from repeated exposures to the carcinogen acriflavine (Stuart, 1971), it is possible that either SCoAS or ASCT accumulated mutations that render it inactive. To verify this scenario, we would need to clone and sequence these DK164 genes. While a plausible experiment, this was not an aim within the limited time frame of this thesis.

Unlike higher eukaryotes, trypanosomes do not regulate the abundance of gene products through transcription (Clayton, 2019). Therefore, the observation of decreased ASCT and SCoAS protein levels in dyskinetoplastic strains indicates that these parasites are trying to limit the activity of these enzymes. Another level of enzyme regulation could occur in the form of post-translational modifications. Interestingly, compared to *T. brucei* wt, *T. evansi* ASCT has two substitutions (S419N and T493A) that result in the loss of amino acid residues that could potentially be phosphorylated. However, two previous studies (Nett, 2009; Urbaniak et al., 2013) that identified the phosphoproteome of BF *T brucei* wt parasites do not indicate that ASCT is phosphorylated under the conditions tested. Alternatively, TriTrypDB indicates that ASCT is acetylated at lysine 396 (Moretti et al., 2018). While nothing is known about the possible mechanisms regulating ASCT activity, the acetylation of lysine residues neutralizes their charge and can alter protein−protein interactions, protein complex formation and enzymatic activities (Choudhary et al., 2014). To determine if there are indeed any ASCT post-translational modifications that can alter the rate of enzymatic activity and potentially further reduce ATP production inthese dyskinetoplastic trypanosomes, several experiments can be proposed. Heterologous expression of the *T. evansi* ASCT could be used to rescue a BF *T. brucei* ΔASCT mutant. Presuming this does not result in a lethal phenotype, the amount of acetate production or the mitochondrial ATP levels could be measured and compared to BF *T. brucei* wt parasites. Any decrease in these outputs would signify that the *T. evansi* ASCT has a lower rate of activity, assuming the abundance of the protein remained constant. In addition, *T. evansi* proteomics or mass spectrophotometry of the purified enzyme could be analyzed for any post-translational modifications.

Maintenance of the mitochondrial membrane potential of dyskinetoplastids is predominantly provided by AAC, which exchanges cytosolic ATP^{4-} derived from glycolysis with mitochondrial ADP^{3-} generated from F_1-ATPase activity. In this manner, AAC creates an electrogenic membrane potential. This dependence on ATP synthase activity is best captured by the fact that the EC_{50} of the F_1 inhibitor, azide, is the same for BF *T. brucei wt* as it is for DK164 (unpublished Zíková lab data). Due to this interconnectivity between various bioenergetic components, we also examined if other proteins had altered expression levels.

Interestingly, AAC expression levels were only significantly reduced in *T. evansi*, which also had the sharpest reductions in the abundance of ASCT and SCoAS. Meanwhile, the abundance of ATP synthase subunit beta was similarly reduced in all dyskinetoplastids compared to *T. brucei* wt. However, to verify that our results are reproducible and statistically significant, these western blot analyses will need to be performed again with biological triplicates. If desired, these results can even be quantified using a scanning densitometry software to more accurately compare any observed changes. Furthermore, our results should consider that ATP synthase is composed of 25 proteins and the steady state abundance of a single denatured subunit is not necessarily a good indicator of the amount of assembled ATP synthase nor its rate of activity. To perform more thorough experiments to compare the amount of assembled ATP synthase complexes, it would be better to use immunoblotting of protein complexes resolved by blue native polyacrylamide gel electrophoresis. Simultaneously, the amount of activity of these same complexes can be compared by in-gel ATP hydrolysis staining methods.

These differences in the expression levels of various bioenergetic components between DK164 and *T. evansi* also suggests that maybe there are different ways for the parasite to adapt to the loss of its mitochondrial genome. This becomes even more pertinent when considering the evolutionary pressure experienced by the DK164 strain as it was generated within months. Another interesting approach to explore this possibility would be to analyze the quantitative proteomics and metabolomics of these two disparate dyskinetoplastic strains.

Even if the reduction of AAC expression levels in *T. evansi* is confirmed in subsequent western blot analyses, this does not give us any indication about the rate or directionality of mitochondrial ATP transport. These characteristics of AAC are determined by two important factors, the ratio of mitochondrial ATP/ADP and the proton motive force (PMF). Normally, the mitochondrion acts as a powerhouse for the cell by producing significant amounts of ATP through oxidative phosphorylation. This chemical energy in the form of ATP is then transported by AAC to the cytosol to meet all the energetic needs of the cell. In this scenario, the ATP synthase and AAC are both working in their forward modes (Figure 17, A). However, if oxidative phosphorylation becomes compromised, either or both of these bioenergetic components can switch to operate in their reverse modes (Figure 17, B-D) (St-Pierre, 2000). In simplistic terms, if the ATP concentration is greater in the cytosol than the mitochondria, AAC will reverse and transport ATP into the mitochondria due to the thermodynamic laws of entropy. Similarly, ATP synthase will reverse and hydrolyze ATP when the ratio of mitochondrial ATP/ADP is high. The PMF is also a significant factor in the calculations predicting when ATP

synthase or AAC will enter their reverse mode. PMF consists of the proton concentration gradient, ΔpH, and the difference in the electrical transmembrane potential ($\Delta\Psi_m$). Typically, the ΔpH of the mitochondrial inner membrane is quite low and the PMF is often denoted as just $\Delta\Psi_m$ (Chinopoulos, 2011). However, this does not apply to all biological membranes, as the ΔpH is quite significant in chloroplasts. If the exact values of the mitochondrial ATP/ADP ratio are known along with the absolute membrane potential measured in mV, they can be entered into an equation (http://www.tinyurl.com/Erev-estimator) to determine if AAC and ATP synthase are operating in the forward or reverse modes (Chinopolous et al., 2010).

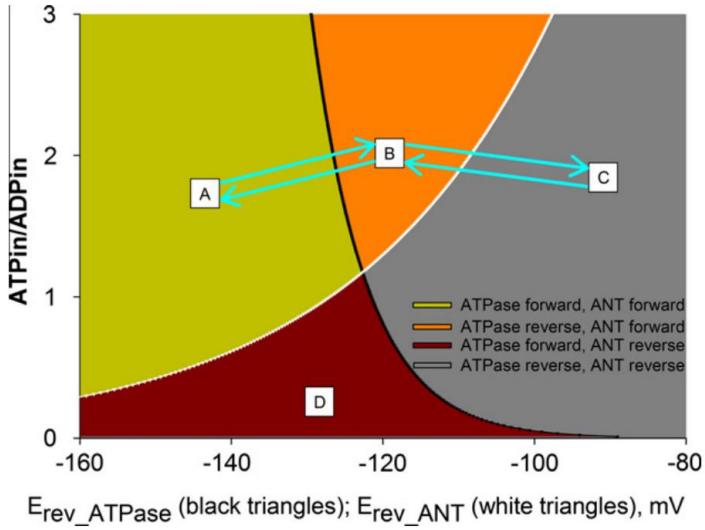

Figure 17: Computational estimations of the boundaries that dictate if the ATP synthase or AAC will operate in the forward or reverse mode. The forward mode is defined as when the ATP synthase generates ATP and when the AAC exchanges mitochondrial ATP for cytosolic ADP. The Y-axis indicates the ratio of ATP/ADP inside the mitochondrial matrix, while the X-axis represents the $\Delta\Psi_m$. (A) The region where the ATP synthase and AAC function in the forward mode. (B) The ATP synthase works in the reverse mode and AAC in the forward mode. (C) The ATP synthase and AAC both work in reverse mode. (D) The ATP synthase operates in forward mode while AAC works in reverse mode. Adapted from Chinopoulos, 2011.

The presence of various *T. brucei* bioenergetic components are regulated by the life cycle stage of the parasite. In PF *T. brucei*, there is canonical oxidative phosphorylation (OXPHOS), with respiratory complex III and IV pumping protons to generate the PMF. ATP synthase operates in the forward mode and uses the PMF to generate ATP in the mitochondrial matrix, which is then redistributed to the cytosol by the forward activity of AAC. It has also been demonstrated that the mitochondria of PF parasites produce ATP via substrate

phosphorylation pathways (Bochud-Allemann & Schneider, 2002). However, BF *T. brucei* lack respiratory complex III and IV and as a result, ATP synthase works in the reverse mode to hydrolyzing ATP to pump protons across the inner mitochondrial membrane. While it was long thought that the BF *T. brucei* mitochondria was only an ATP-consuming organelle, there is now growing evidence that substrate phosphorylation also occurs in this life stage (Mochizuki et al., 2020; Zíková, 2023, unpublished). This unknown amount of mitochondrial ATP synthesized via substrate phosphorylation is thought to provide the substrate for the reverse activity of the ATP synthase. Although it has been estimated how much ATP would be required to maintain the BF *T. brucei* mitochondrial membrane potential (Nascimento et al., 2023), we do not yet know what are the rates of mitochondrial substrate phosphorylation, the rate of ATP hydrolysis by the ATP synthase, nor the rate or direction of AAC. However, research on this topic is currently ongoing in the lab.

In some respects, more of the bioenergetic factors are known for dyskinetoplastic trypanosomes. Although the rate of mitochondrial ATP import and hydrolysis are still unknown, we know that AAC and ATP synthase both function in their reverse modes (Šubrtová et al., 2015, Procházková et al., 2018). Furthermore, while BF *T. brucei* are quite resistant to the AAC inhibitor, carboxyatractyloside, dyskinetoplastic strains are drastically more sensitive to the drug (Procházková et al., 2018). Presumably, this is because dyskinetoplastids utterly rely on AAC to operate in the reverse mode to maintain the essential mitochondrial membrane potential. Therefore, the observed intermediate growth phenotype that coincided with the decreased mitochondrial membrane potential when ASCT expression was forcibly induced in the DK164 strain, indicates that the level of mitochondrial substrate phosphorylation must be kept to a minimum in dyskinetoplastids. In fact, when ASCT expression was induced in *T. evansi*, where the levels of endogenous ASCT was almost undetectable by western blot analysis, the parasites initially became cytostatic. Since we lost the ability to induce protein expression in this strain, the ASCT *T. evansi* cell line will have to be generated again and further characterized. Only then will we confirm that triggering higher levels of mitochondrial substrate phosphorylation in the naturally occurring dyskinetoplastids is debilitating. Even the mitochondrial membrane potential measurements for the ASCT DK164 cell line will need to be repeated as the dramatic decrease between then noninduced ASCT cell line and the parental DK164 wt cells was surprising. Normally, such an overall decrease would predict a much more severe growth phenotype, similar to that observed in the ASCT *T. evansi* cell line. However,

this could be partially explained by the small amount of leaky ASCT expression detected by western blot analyse in the noninduced DK164 ASCT cell line.

The exciting preliminary results presented in this thesis support our hypothesis that dyskinetoplastic mitochondrial ATP synthesis by substrate phosphorylation must be limited so as not to interrupt the rate and/or directionality of AAC. Several future experiments will help to solidify our initial interpretation of the data. To demonstrate that ASCT overexpression in dyskinetoplastids does increase substrate phosphorylation, a total cellular ATP measurement using a kit or an analytical method using mass spectrometry could be performed. Additionally, the dyskinetoplastic ASCT cell line can be transfected with a luciferase targeted to the mitochondrion, which can then be used to more sensitively measure *in vivo* mitochondrial ATP levels. Finally, to more accurately measure the mitochondrial membrane potential of DK164 ASCT compared to the parental DK164 wt, the OROBOROS instrument with a fluorimeter can be used to quantify the TMRE fluorescence when the cell line is titrated with the FCCP ionophore.

6. References

Allmann, S., & Bringaud, F. (2017). Glycosomes: A comprehensive view of their metabolic roles in T. brucei. *The international journal of biochemistry & cell biology*, *85*, 85–90. https://doi.org/10.1016/j.biocel.2017.01.015

Bílý, T., Sheikh, S., Mallet, A., Bastin, P., Pérez-Morga, D., Lukeš, J., & Hashimi, H. (2021). Ultrastructural Changes of the Mitochondrion During the Life Cycle of Trypanosoma brucei. *The Journal of eukaryotic microbiology*, *68*(3), e12846. https://doi.org/10.1111/jeu.12846

Bochud-Allemann, N., & Schneider, A. (2002). Mitochondrial substrate level phosphorylation is essential for growth of procyclic Trypanosoma brucei. *The Journal of biological chemistry*, *277*(36), 32849–32854. https://doi.org/10.1074/jbc.M205776200

Borst, P., Fase-Fowler, F., & Gibson, W. C. (1987). Kinetoplast DNA of Trypanosoma evansi. *Molecular and biochemical parasitology*, *23*(1), 31–38. https://doi.org/10.1016/0166-6851(87)90184-8

Borst, P., & Hoeijmakers, J. H. (1979). Kinetoplast DNA. *Plasmid*, *2*(1), 20–40. https://doi.org/10.1016/0147-619x(79)90003-9

Büscher, P., Cecchi, G., Jamonneau, V., & Priotto, G. (2017). Human African trypanosomiasis. *Lancet (London, England)*, *390*(10110), 2397–2409. https://doi.org/10.1016/S0140-6736(17)31510-6

Carnes, J., Anupama, A., Balmer, O., Jackson, A., Lewis, M., Brown, R., Cestari, I., Desquesnes, M., Gendrin, C., Hertz-Fowler, C., Imamura, H., Ivens, A., Kořený, L., Lai, D. H., MacLeod, A., McDermott, S. M., Merritt, C., Monnerat, S., Moon, W., Myler, P., … Schnaufer, A. (2015). Genome and phylogenetic analyses of Trypanosoma evansi reveal extensive similarity to T. brucei and multiple independent origins for dyskinetoplasty. *PLoS neglected tropical diseases*, *9*(1), e3404. https://doi.org/10.1371/journal.pntd.0003404

Chaudhuri, M., Ott, R. D., & Hill, G. C. (2006). Trypanosome alternative oxidase: from molecule to function. *Trends in parasitology*, *22*(10), 484–491. https://doi.org/10.1016/j.pt.2006.08.007

Chinopoulos C. (2011). Mitochondrial consumption of cytosolic ATP: not so fast. *FEBS letters, 585(9)*, 1255–1259. https://doi.org/10.1016/j.febslet.2011.04.004

Chinopoulos, C., Gerencser, A. A., Mandi, M., Mathe, K., Töröcsik, B., Doczi, J., Turiak, L., Kiss, G., Konràd, C., Vajda, S., Vereczki, V., Oh, R. J., & Adam-Vizi, V. (2010). Forward operation of adenine nucleotide translocase during F0F1-ATPase reversal: critical role of matrix substrate-level phosphorylation. *FASEB journal: official publication of the Federation of American Societies for Experimental Biology*, *24*(7), 2405–2416. https://doi.org/10.1096/fj.09-149898

Chong, Z. X., Yeap, S. K., & Ho, W. Y. (2021). Transfection types, methods and strategies: a technical review. *PeerJ*, *9*, e11165. https://doi.org/10.7717/peerj.11165

Choudhary, V., Darwiche, R., Gfeller, D., Zoete, V., Michielin, O., & Schneiter, R. (2014). The caveolin-binding motif of the pathogen-related yeast protein Pry1, a member of the CAP protein superfamily, is required for in vivo export of cholesteryl acetate. *Journal of lipid research*, *55*(5), 883–894. https://doi.org/10.1194/jlr.M047126

Claes, F., Büscher, P., Touratier, L., & Goddeeris, B. M. (2005). Trypanosoma equiperdum: master of disguise or historical mistake?. *Trends in parasitology*, *21*(*7*), 316–321. https://doi.org/10.1016/j.pt.2005.05.010

Clayton C. (2019). Regulation of gene expression in trypanosomatids: living with polycistronic transcription. *Open biology*, *9*(6), 190072. https://doi.org/10.1098/rsob.190072

Crowley, L. C., Christensen, M. E., & Waterhouse, N. J. (2016). Measuring Survival of Adherent Cells with the Colony-Forming Assay. *Cold Spring Harbor protocols*, *2016*(8), 10.1101/pdb.prot087171. https://doi.org/10.1101/pdb.prot087171

Dean, S., Gould, M. K., Dewar, C. E., & Schnaufer, A. C. (2013). Single point mutations in ATP synthase compensate for mitochondrial genome loss in trypanosomes. *Proceedings of the National Academy of Sciences of the United States of America*, *110*(36), 14741–14746. https://doi.org/10.1073/pnas.1305404110

Desquesnes, M., Holzmuller, P., Lai, D. H., Dargantes, A., Lun, Z. R., & Jittaplapong, S. (2013). Trypanosoma evansi and surra: a review and perspectives on origin, history, distribution, taxonomy, morphology, hosts, and pathogenic effects. *BioMed research international*, *2013*, 194176. https://doi.org/10.1155/2013/194176

Dickie, E. A., Giordani, F., Gould, M. K., Mäser, P., Burri, C., Mottram, J. C., Rao, S. P. S., & Barrett, M. P. (2020). New Drugs for Human African Trypanosomiasis: A Twenty First Century Success Story. *Tropical medicine and infectious disease*, *5*(1), 29. https://doi.org/10.3390/tropicalmed5010029

DNA Ligase, T4 - Worthington Enzyme Manual. (2023, March 15). Worthington Biochemical. https://www.worthington-biochem.com/products/dna-ligase-t4/manual

Domingo, G. J., Palazzo, S. S., Wang, B., Pannicucci, B., Salavati, R., & Stuart, K. D. (2003). Dyskinetoplastic Trypanosoma brucei contains functional editing complexes. *Eukaryotic cell*, *2*(3), 569–577. https://doi.org/10.1128/EC.2.3.569-577.2003

Gel electrophoresis. (2023, March 13). Khan Academy. https://www.khanacademy.org/science/ap-biology/gene-expression-and-regulation/biotechnology/a/gel-electrophoresis

General guidelines for primer design. (2015). MIT OpenCourseWare. https://ocw.mit.edu/courses/7-15-experimental-molecular-genetics-spring-2015/b6d9befecddfc6f51fc98157769dceaa_MIT7_15S15_Primer_design.pdf

Horn D. (2022). A profile of research on the parasitic trypanosomatids and the diseases they cause. *PLoS neglected tropical diseases*, *16*(1), e0010040. https://doi.org/10.1371/journal.pntd.0010040

Human African trypanosomiasis (sleeping sickness). (2023, March 12). World Health Organization. https://www.who.int/health-topics/human-african-trypanosomiasis

Husová, M. (2021). Elucidating the source of bloodstream Trypanosoma brucei mitochondrial ATP. Mgr. Thesis, in English. – 74 p., Faculty of Science, University of South Bohemia, České Budějovice, Czech Republic

Johnston, K., Kim, D. H., Kerkhoven, E. J., Burchmore, R., Barrett, M. P., & Achcar, F. (2019). Mapping the metabolism of five amino acids in bloodstream form *Trypanosoma brucei* using U-^{13}C-labelled substrates and LC-MS. *Bioscience reports*, *39*(5), BSR20181601. https://doi.org/10.1042/BSR20181601

Kaufer, A., Ellis, J., Stark, D., & Barratt, J. (2017). The evolution of trypanosomatid taxonomy. *Parasites & vectors*, *10*(1), 287. https://doi.org/10.1186/s13071-017-2204-7

KOD Hot Start DNA Polymerase (2023, March 13). https://www.merckmillipore.com/CZ/cs/product/KOD-Hot-Start-DNA-Polymerase,EMD_BIO-71086#anchor_USP

Langousis, G., & Hill, K. L. (2014). Motility and more: the flagellum of Trypanosoma brucei. *Nature reviews. Microbiology*, *12*(7), 505–518. https://doi.org/10.1038/nrmicro3274

Lukeš, J., Kachale, A., Votýpka, J., Butenko, A., & Field, M. C. (2022). African trypanosome strategies for conquering new hosts and territories: the end of monophyly?. *Trends in parasitology*, *38*(9), 724–736. https://doi.org/10.1016/j.pt.2022.05.011

Lun, Z. R., Brun, R., & Gibson, W. (1992). Kinetoplast DNA and molecular karyotypes of Trypanosoma evansi and Trypanosoma equiperdum from China. *Molecular and*

biochemical parasitology, *50*(2), 189–196. https://doi.org/10.1016/0166-6851(92)90215-6

Mahmood, T., & Yang, P. C. (2012). Western blot: technique, theory, and trouble shooting. *North American journal of medical sciences*, *4*(9), 429–434. https://doi.org/10.4103/1947-2714.100998

Mantilla, B. S., Marchese, L., Casas-Sánchez, A., Dyer, N. A., Ejeh, N., Biran, M., Bringaud, F., Lehane, M. J., Acosta-Serrano, A., & Silber, A. M. (2017). Proline Metabolism is Essential for Trypanosoma brucei brucei Survival in the Tsetse Vector. *PLoS pathogens*, *13*(1), e1006158. https://doi.org/10.1371/journal.ppat.1006158

Matthews K. R. (2021). Trypanosome Signaling-Quorum Sensing. *Annual review of microbiology*, *75*, 495–514. https://doi.org/10.1146/annurev-micro-020321-115246

Mazet, M., Morand, P., Biran, M., Bouyssou, G., Courtois, P., Daulouède, S., Millerioux, Y., Franconi, J. M., Vincendeau, P., Moreau, P., & Bringaud, F. (2013). Revisiting the central metabolism of the bloodstream forms of Trypanosoma brucei: production of acetate in the mitochondrion is essential for parasite viability. *PLoS neglected tropical diseases*, *7*(12), e2587. https://doi.org/10.1371/journal.pntd.0002587

Michels, P. A. M., Villafraz, O., Pineda, E., Alencar, M. B., Cáceres, A. J., Silber, A. M., & Bringaud, F. (2021). Carbohydrate metabolism in trypanosomatids: New insights revealing novel complexity, diversity and species-unique features. *Experimental parasitology*, *224*, 108102. https://doi.org/10.1016/j.exppara.2021.108102

Mochizuki, K., Inaoka, D. K., Mazet, M., Shiba, T., Fukuda, K., Kurasawa, H., Millerioux, Y., Boshart, M., Balogun, E. O., Harada, S., Hirayama, K., Bringaud, F., & Kita, K. (2020). The ASCT/SCS cycle fuels mitochondrial ATP and acetate production in Trypanosoma brucei. *Biochimica et biophysica acta. Bioenergetics*, *1861*(11), 148283. https://doi.org/10.1016/j.bbabio.2020.148283

Moretti, N. S., Cestari, I., Anupama, A., Stuart, K., & Schenkman, S. (2018). Comparative proteomic analysis of lysine acetylation in trypanosomes. *Journal of Proteome Research*, *17*(1), 374–385. https://doi.org/10.1021/acs.jproteome.7b00603

Mugnier, M. R., Stebbins, C. E., & Papavasiliou, F. N. (2016). Masters of Disguise: Antigenic Variation and the VSG Coat in Trypanosoma brucei. *PLoS pathogens*, *12*(9), e1005784. https://doi.org/10.1371/journal.ppat.1005784

Nascimento, J. F., Souza, R. O. O., Alencar, M. B., Marsiccobetre, S., Murillo, A. M., Damasceno, F. S., Girard, R. B. M. M., Marchese, L., Luévano-Martinez, L. A., Achjian, R. W., Haanstra, J. R., Michels, P. A. M., & Silber, A. M. (2023). How much (ATP) does it cost to build a trypanosome? A theoretical study on the quantity of ATP needed to maintain and duplicate a bloodstream-form Trypanosoma brucei cell. https://doi.org/10.1101/2023.03.07.531645

Neikov, O.D., & Yefimov, N.A. (2019). Powder Characterization and Testing. *Handbook of Non-Ferrous Metal Powders*. https://doi.org/ 10.1016/b978-0-08-100543-9.00001-4

Nett, I. R., Martin, D. M., Miranda-Saavedra, D., Lamont, D., Barber, J. D., Mehlert, A., & Ferguson, M. A. (2009). The phosphoproteome of bloodstream form Trypanosoma brucei, causative agent of African sleeping sickness. *Molecular & cellular proteomics : MCP*, *8*(7), 1527–1538. https://doi.org/10.1074/mcp.M800556-MCP200

Okello, I., Mafie, E., Eastwood, G., Nzalawahe, J., & Mboera, L. E. G. (2022). African Animal Trypanosomiasis: A Systematic Review on Prevalence, Risk Factors and Drug Resistance in Sub-Saharan Africa. *Journal of medical entomology*, *59*(4), 1099–1143. https://doi.org/10.1093/jme/tjac018

One Health. (2023, March 12). University of Glasgow. https://www.gla.ac.uk/research/beacons/onehealth/morefeatures/animalafricantrypanosomiasis/

Podlipaev S. (2001). The more insect trypanosomatids under study-the more diverse Trypanosomatidae appears. *International journal for parasitology*, *31*(5-6), 648–652. https://doi.org/10.1016/s0020-7519(01)00139-4

Polymerase Chain Reaction (PCR). (2023, March 13). Genome.gov. https://www.genome.gov/genetics-glossary/Polymerase-Chain-Reaction

Primer Designing - Demonstration step by step. (2023, March 13). Sharebiology. https://sharebiology.com/primer-designing-demonstration-step-by-step/

Procházková, M., Panicucci, B. & Zíková, A. Cultured bloodstream *Trypanosoma brucei* adapt to life without mitochondrial translation release factor 1. *Sci Rep* **8**, 5135 (2018). https://doi.org/10.1038/s41598-018-23472-6

Restriction enzymes & DNA ligase (2023, March 15). Khan Academy. https://www.khanacademy.org/science/biology/biotech-dna-technology/dna-cloning-tutorial/a/restriction-enzymes-dna-ligase

Rivière, L., Moreau, P., Allmann, S., Hahn, M., Biran, M., Plazolles, N., Franconi, J. M., Boshart, M., & Bringaud, F. (2009). Acetate produced in the mitochondrion is the essential precursor for lipid biosynthesis in procyclic trypanosomes. *Proceedings of the National Academy of Sciences of the United States of America*, *106*(31), 12694–12699. https://doi.org/10.1073/pnas.0903355106

Schnaufer, A., Clark-Walker, G. D., Steinberg, A. G., & Stuart, K. (2005). The F1-ATP synthase complex in bloodstream stage trypanosomes has an unusual and essential function. *The EMBO journal*, *24*(23), 4029–4040. https://doi.org/10.1038/sj.emboj.7600862

Schneider A. (2001). Unique aspects of mitochondrial biogenesis in trypanosomatids. *International journal for parasitology*, *31*(13), 1403–1415. https://doi.org/10.1016/s0020-7519(01)00296-x

Shlomai J. (2004). The structure and replication of kinetoplast DNA. Current molecular medicine, 4(6), 623–647. https://doi.org/10.2174/1566524043360096

Silvester, E., McWilliam, K. R., & Matthews, K. R. (2017). The Cytological Events and Molecular Control of Life Cycle Development of Trypanosoma brucei in the Mammalian Bloodstream. *Pathogens (Basel, Switzerland)*, *6*(3), 29. https://doi.org/10.3390/pathogens6030029

Simpson, A. G., Stevens, J. R., & Lukes, J. (2006). The evolution and diversity of kinetoplastid flagellates. *Trends in parasitology*, *22*(4), 168–174. https://doi.org/10.1016/j.pt.2006.02.006

St-Pierre, J., Brand, M. D., & Boutilier, R. G. (2000). Mitochondria as ATP consumers: cellular treason in anoxia. *Proceedings of the National Academy of Sciences of the United States*

of America, *97*(15), 8670–8674. https://doi.org/10.1073/pnas.140093597

Stuart K. D. (1971). Evidence for the retention of kinetoplast DNA in an acriflavine-induced dyskinetoplastic strain of Trypanosoma brucei which replicates the altered central element of the kinetoplast. *The Journal of cell biology*, *49*(1), 189–195. https://doi.org/10.1083/jcb.49.1.189

Stuart, K. D., Schnaufer, A., Ernst, N. L., & Panigrahi, A. K. (2005). Complex management: RNA editing in trypanosomes. *Trends in biochemical sciences*, *30*(2), 97–105. https://doi.org/10.1016/j.tibs.2004.12.006

Swallow, B. M. (2000). Impacts of Trypanosomiasis on African Agriculture (PAAT Technical and Scientific Series 2). Food and Agriculture Organization.

Šubrtová, K., Panicucci, B., & Zíková, A. (2015). ATPaseTb2, a unique membrane-bound FoF1-ATPase component, is essential in bloodstream and dyskinetoplastic trypanosomes. *PLoS pathogens*, *11*(2), e1004660. https://doi.org/10.1371/journal.ppat.1004660

Urbaniak, M. D., Martin, D. M., & Ferguson, M. A. (2013). Global quantitative SILAC phosphoproteomics reveals differential phosphorylation is widespread between the procyclic and bloodstream form lifecycle stages of Trypanosoma brucei. *Journal of proteome research*, *12*(5), 2233–2244. https://doi.org/10.1021/pr400086y

Van Hellemond, J. J., Opperdoes, F. R., & Tielens, A. G. (1998). Trypanosomatidae produce acetate via a mitochondrial acetate:succinate CoA transferase. *Proceedings of the National Academy of Sciences of the United States of America*, *95*(6), 3036–3041. https://doi.org/10.1073/pnas.95.6.3036

Verner, Z., Basu, S., Benz, C., Dixit, S., Dobáková, E., Faktorová, D., Hashimi, H., Horáková, E., Huang, Z., Paris, Z., Peña-Diaz, P., Ridlon, L., Týč, J., Wildridge, D., Zíková, A., & Lukeš, J. (2015). Malleable mitochondrion of Trypanosoma brucei. *International review of cell and molecular biology*, *315*, 73–151. https://doi.org/10.1016/bs.ircmb.2014.11.001

Williams, C. F. (2022). Microbial Metabolism. In Encyclopedia of Infection and Immunity (pp. 363–376). https://doi.org/10.1016/b978-0-12-818731-9.00188-9

Zíková A. (2022). Mitochondrial adaptations throughout the Trypanosoma brucei life cycle. *The Journal of eukaryotic microbiology*, *69*(6), e12911. https://doi.org/10.1111/jeu.12911

Zíková, A., Verner, Z., Nenarokova, A., Michels, P. A. M., & Lukeš, J. (2017). A paradigm shift: The mitoproteomes of procyclic and bloodstream Trypanosoma brucei are comparably complex. *PLoS pathogens*, *13*(12), e1006679. https://doi.org/10.1371/journal.ppat.1006679